

---

# RobFR: Benchmarking Adversarial Robustness on Face Recognition

---

Xiao Yang, Dingcheng Yang, Yinpeng Dong, Hang Su, Wenjian Yu, Jun Zhu  
Department of Computer Science & Technology, Tsinghua University, Beijing, China  
{yangxiao19, ydc19, dyp17}@mails.tsinghua.edu.cn, {suhangss, yu-wj, dcszj}@tsinghua.edu.cn

## Abstract

Face recognition (FR) has recently made substantial progress and achieved high accuracy on standard benchmarks. However, it has raised security concerns in enormous FR applications because deep CNNs are unusually vulnerable to adversarial examples, and it is still lack of a comprehensive robustness evaluation before a FR model is deployed in safety-critical scenarios. To facilitate a better understanding of the adversarial vulnerability on FR, we develop an adversarial robustness evaluation library on FR named **RobFR**, which serves as a reference for evaluating the robustness of downstream tasks. Specifically, RobFR involves 15 popular naturally trained FR models, 9 models with representative defense mechanisms and 2 commercial FR API services, to perform the robustness evaluation by using various adversarial attacks as an important surrogate. The evaluations are conducted under diverse adversarial settings in terms of dodging and impersonation,  $\ell_2$  and  $\ell_\infty$ , as well as white-box and black-box attacks. We further propose a landmark-guided cutout (LGC) attack method to improve the transferability of adversarial examples for black-box attacks by considering the special characteristics of FR. Based on large-scale evaluations, the commercial FR API services fail to exhibit acceptable performance on robustness evaluation, and we also draw several important conclusions for understanding the adversarial robustness of FR models and providing insights for the design of robust FR models. RobFR is open-source and maintains all extendable modules, i.e., *Datasets*, *FR Models*, *Attacks&Defenses*, and *Evaluations* at <https://github.com/ShawnXYang/Face-Robustness-Benchmark>, which will be continuously updated to promote future research on robust FR.

## 1 Introduction

Automatic face recognition (FR) is becoming a prevalent authentication solution in numerous biometric applications aiming to identify or verify a person from visual images. Recent progress in deep convolutional neural networks (CNNs) together with the use of abundant data [15, 38, 42] has greatly facilitated the massive development of FR algorithms [40, 43], which have demonstrated the state-of-the-art performance by incorporating the margin-based loss functions [5, 25, 33, 47, 48] into deep CNN architectures. The excellent performance allows the FR models to be widely deployed in diverse scenarios ranging from financial payment to automated border control systems.

Recent research in adversarial machine learning has revealed that deep CNNs are highly vulnerable to adversarial examples [13, 41, 55], which are generated by adding a small amount of distortion to an image. FR systems based on deep CNNs inherit such vulnerability to adversarial examples. Considering that FR is generally safety-critical, there may exist a malicious party aiming at misleading the FR systems to achieve an illegal purpose. For example, an adversary can evade being recognized or impersonate another identity by wearing an adversarial eyeglass [36, 37, 54]. Some commercial FR API services can be attacked by the adversarial examples in the black-box manner [10]. As a result, adversarial attacks raise security issues to the FR systems in real-world task-critical applications,

e.g., a facial payment system. It is therefore imperative to conduct a comprehensive and rigorous evaluation for a FR model before it is deployed. Although numerous enhanced methods [8, 23, 29, 31] have been proposed to conduct evaluation on image classification, it is still lack of a comprehensive evaluation on FR.

Compared with the evaluation of adversarial robustness on the conventional image classification task, benchmarking adversarial robustness on FR remains as a challenging task. First, FR models usually have more elaborate losses since FR requires to enhance high inter-class diversity and intra-class similarity simultaneously. It has witnessed various loss functions, e.g., Euclidean-distance-based losses [33, 40, 48] and angular-margin-based losses [5, 25, 47]. Second, as a pioneering application in the vision tasks, the architectures for FR are richer and diversified in that numerous attempts have been made to modify mainstream architectures [6, 25] for the adaptiveness in FR or develop assembled networks [18]. Therefore, when facing FR task with more diverse loss functions and network architectures, we still lack an in-depth understanding on whether there exists any correlation between the robustness and accuracy of the current FR models. Thus it is of significant importance to benchmark the adversarial robustness of the existing FR models under various settings. It will guide the users to choose proper models for different applications, and facilitate a better understanding of their robustness, which provides insights for the design of more robust models in facial tasks.

In this paper, we establish a comprehensive and rigorous evaluation method of the adversarial robustness on FR, including white-box and black-box attack settings based on various representative FR models, covering diverse network architectures, training objectives, and defense mechanisms. We consider face verification, an important sub-domain of face recognition aiming at distinguishing whether a pair of facial images belong to the same identity [13], since it has a standard well-defined testing protocol for the comparison between different algorithms but can also provide a good reference for other sub-tasks, e.g., face identification. Specifically, we incorporate 15 popular naturally trained FR models, which cover most of the models trained by representative losses and network architectures. We also involve 9 representative defense models including input transformation [12, 52] and adversarial training [1] in the FR task for the first time. we adopt several evaluation metrics, including 1) attack success rate (Asr); 2) *Asr vs. perturbation budget robustness* curves that can give a global understanding of the robustness of FR models; 3) transfer-based Asr that can directly reflect black-box evaluation results by using adversarial examples generated against a substitute model. Moreover, we carry out large-scale experiments under thorough threat models to fully demonstrate the performance of different FR models, including 1) dodging and impersonation attacks; 2)  $\ell_2$  and  $\ell_\infty$  attacks; 3) white-box and black-box attacks that can reflect the evaluation results in different levels. Thus they are recommended as the robustness evaluation metrics for future works on FR.

Since the existing adversarial libraries (e.g., CleverHans [29], Foolbox [31], FACESEC [44], ARES [11]) cannot fully support our evaluations in FR (see Appendix A). In this paper, we develop a new adversarial robustness evaluation library on face recognition named **RobFR** to conduct all experiments. RobFR consists of four modules, *i.e.*, Datasets, FR Models, Attacks & Defenses, and Evaluations, which takes a easily extendable implementation due to independent interface, thus enabling more researchers to conveniently supplement new contents. In RobFR we further propose a *landmark-guided cutout* (LGC) attack method in RobFR to improve the performance of black-box attacks by considering the particular characteristics of FR. LGC can be flexibly incorporated into black-box attack methods to improve their performances, such as MIM [8], DIM [51], and TIM [9].

By analyzing the evaluation results, we have some important findings. First, the excellent algorithms with glorious precision in FR, e.g., ArcFace [6] and CosFace [47], fail to substantially improve the robustness. Considering the safety-critical requirement, future FR research should significantly take into account the robustness when pursuing a high precision. Second, model architecture is a more critical factor for boosting robustness than other factors, e.g., loss functions. Thus selecting a proper larger network structure as a backbone usually exhibits better resistance against adversarial examples, which also provides an insight of designing robust FR models for the future. Third, adversarial training (AT) is the most robust method among the various defense methods, whereas AT results in a degeneration of natural accuracy and high training cost. More discussions are provided in Sec. 4.3.

## 2 Background and Threat Models

Let  $f(\mathbf{x}) : \mathcal{X} \rightarrow \mathbb{R}^d$  denote a FR model that extracts a normalized feature representation in  $\mathbb{R}^d$  for an input face image  $\mathbf{x} \in \mathcal{X} \subset \mathbb{R}^n$ . Face verification aims to compute the distance between the feature

representations of image pair  $\{\mathbf{x}_1, \mathbf{x}_2\} \subset \mathcal{X}$ . We first denote their feature distance  $\mathcal{D}_f(\mathbf{x}_1, \mathbf{x}_2)$  as

$$\mathcal{D}_f(\mathbf{x}_1, \mathbf{x}_2) = \|f(\mathbf{x}_1) - f(\mathbf{x}_2)\|_2^2. \quad (1)$$

Face verification can therefore be formally formulated as

$$\mathcal{C}(\mathbf{x}_1, \mathbf{x}_2) = \mathbb{I}(\mathcal{D}_f(\mathbf{x}_1, \mathbf{x}_2) < \delta), \quad (2)$$

where  $\mathbb{I}$  is the indicator function, and  $\delta$  is a threshold. When  $\mathcal{C}(\mathbf{x}_1, \mathbf{x}_2)$  equals to 1, the image pair is recognized as the same identity and otherwise different identities. Notely, this definition is consistent with the commonly used cosine similarity metric, since  $f$  usually outputs a normalized vector.

Given a FR model, we need to specify the threat models for robustness evaluation, including different goals, capabilities, and knowledge [3] of the adversary.

**Adversary’s goals.** We focus on two types of attacks in terms dodging and impersonation. Specifically, *dodging attacks* seeks to mislead a face recognition system thus have one face misidentified. In general, dodging attacks are of great interests in evading surveillance. Formally, given a pair of face images  $\mathbf{x}$  and  $\mathbf{x}^r$  with the *same* identity, the adversary seeks to modify  $\mathbf{x}$  to generate an adversarial image  $\mathbf{x}^{adv}$  that cannot be recognized by the model, i.e., to make  $\mathcal{C}(\mathbf{x}^{adv}, \mathbf{x}^r) = 0$ . On the other hand, *impersonation attacks* aim to generate an adversarial example that can be recognized as a specific victim’s identity, which generally harder than dodging. One attackers can leverage this method to evade the face authentication systems. Formally, given a pair of face images  $\mathbf{x}$  and  $\mathbf{x}^r$  with two *different* identities, the adversary tries to find an adversarial image  $\mathbf{x}^{adv}$  that is recognized as the target identity of  $\mathbf{x}^r$ , i.e., to make  $\mathcal{C}(\mathbf{x}^{adv}, \mathbf{x}^r) = 1$ .

**Adversary’s capabilities.** As adversarial examples are usually assumed to be indistinguishable from the corresponding original ones from human observations [13, 41], the adversary can only introduce small changes to the inputs. In this paper, we study widely used  $\ell_p$  additive perturbation setting, where the adversary is allowed to add a small perturbation measured by the  $\ell_\infty$  and  $\ell_2$  norms to the original input. To achieve the adversary’s goal, we optimize the feature distance between the adversarial image  $\mathbf{x}^{adv}$  and the counterpart face image  $\mathbf{x}^r$ , meanwhile, we keep a small distance between  $\mathbf{x}^{adv}$  and  $\mathbf{x}$  in the input space. For dodging attacks, an adversarial image is generated by maximizing the distance between  $\mathbf{x}'$  and  $\mathbf{x}^r$  in the feature space as

$$\mathbf{x}^{adv} = \arg \max_{\mathbf{x}': \|\mathbf{x}' - \mathbf{x}\|_p \leq \epsilon} \mathcal{D}_f(\mathbf{x}', \mathbf{x}^r), \quad (3)$$

where  $\epsilon$  is a small constant. By solving the problem in Eq. (3), the FR model will misclassify them as different identities when the feature distance is larger than a predefined threshold  $\delta$ . For impersonation attacks, we can formulate the problem as minimizing the distance between  $\mathbf{x}'$  and  $\mathbf{x}^r$  as

$$\mathbf{x}^{adv} = \arg \min_{\mathbf{x}': \|\mathbf{x}' - \mathbf{x}\|_p \leq \epsilon} \mathcal{D}_f(\mathbf{x}', \mathbf{x}^r). \quad (4)$$

Therefore, the feature representation of  $\mathbf{x}^{adv}$  will resemble that of  $\mathbf{x}^r$ , such that they are recognized as the same identity by FR model.

**Adversary’s knowledge.** An adversary can have different levels of knowledge of the target FR models to craft adversarial examples. Besides the white-box access to the model information, the black-box scenario is another important setting to evaluate the robustness in FR, since the black-box attack setting is more practical in real-world applications, e.g., breaking into a commercial FR API. Thus we consider both *white-box attacks* and *black-box attacks* in this paper. White-box attacks rely on detailed information of the target FR model, including architectures, parameters, and gradients of the loss w.r.t. the input. Black-box attacks can be realized based on the transferability of adversarial examples [30]. Transfer-based black-box attacks do not rely on model information but assume the availability of a substitute model based on which the adversarial examples can be generated.

### 3 Benchmarking Adversarial Robustness on Face Recognition

The existing adversarial machine learning platforms, including CleverHans [29], Foolbox [31], ARES [11], etc., focus on the robustness evaluation in image classification. As a comparison, RobFR implements a comprehensive robustness evaluation in FR as illustrated in Fig. 1, which consists of four modules, i.e., Datasets, FR Models, Attacks & Defenses, and Evaluations. Notably, our library takes an easily extendable implementation for every module due to independent interface, thus enabling more researchers to conveniently supplement new contents.

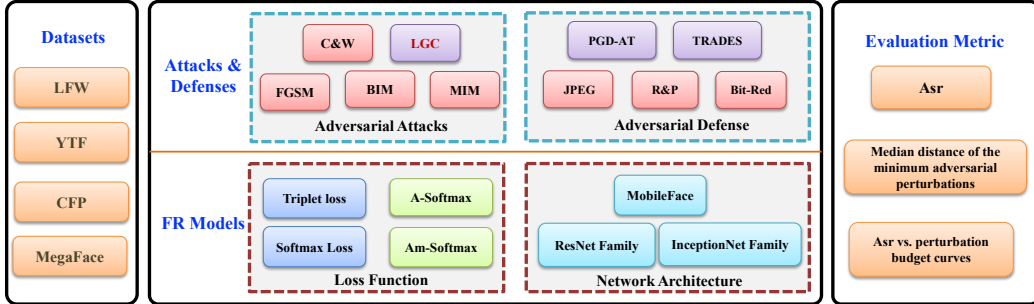


Figure 1: The overall framework of RobFR library. The module of **Datasets** considers current mainstream and more challenging datasets, to perform robustness evaluations. The module of **FR Models** includes 15 representative and popular FR models, covering different *model architectures* including mainstream architectures (e.g., ResNet and InceptionNet families) and light-weight networks (e.g., MobileFace), and *training loss functions* including Euclidean-distance-based losses (e.g., Softmax and Triplet loss) and angular-margin-based losses (e.g., A-Softmax and AM-Softmax). The module of **Attacks & Defenses** incorporates some representative attack and defense algorithms to adapt the FR task. Attacks include *white-box* ones, such as gradient-based FGSM, BIM and MIM and optimization-based C&W, and *black-box* ones, such as FGSM, BIM, MIM and LGC proposed by us. Defenses incorporate two general and representative categories, including *input transformation*, such as JPEG compression, R&P and bit-depth reduction, and *adversarial training*, such as PGD-AT and TRADES. The module of **Evaluation Metric** develops three metrics to evaluate adversarial robustness in FR.

### 3.1 FR Models

To effectively evaluate the robustness of FR models, we choose 15 representative and state-of-the-art FR models, covering different model architectures and training loss functions, as shown in Tab. 1. We first include the best publicly available models FaceNet [33], SphereFace [25], CosFace [47], and ArcFace [6] for evaluations. Besides, to measure the effects of model architectures, we train many models under different backbones with multiple sizes of weights, such as the mainstream architecture ResNet50 [16], and light-weight networks including MobileFace [4], MobileNet [17], MobileNetV2 [32], ShuffleNetV1 [59], and ShuffleNetV2 [26], which are trained by the advanced LMCL loss. Moreover, to study the effects of different training loss functions, we include the models of the same evolved IResNet50 [6] architecture in FR optimized by distance-based losses, such as Softmax, and those optimized by angular-margin-based losses, such as Sphereface, AM-Softmax, CosFace, and ArcFace. We also involve two commercial API services (see Appendix E), and the working mechanism and training data are completely unknown for us. For each model used in our evaluations, we first compute the optimal threshold<sup>1</sup> in Eq. (2) of every FR model by following the standard protocol from the LFW dataset, as shown in Tab. 1. If the distance of two images that are fed into the model exceeds the threshold, we regard them as different identities, otherwise same identities.

### 3.2 Datasets

LFW [19] and YTF [49] are two of the most widely used benchmark datasets for face verification on images and videos. Thus we elaborate the testing protocols via dodging and impersonation attacks to adaptively benchmark the adversarial robustness in FR models. Besides, to further explore robustness evaluations on more challenging datasets, we also perform the evaluation on CFP-FP [35] and MegaFace [20]. Due to numerous individuals from MegaFace, in this study we randomly choose 6,000 pairs to implement the robustness evaluation from standard verification protocols.

<sup>1</sup>The Euclidean threshold  $\delta_d$  can be obtained from the Cosine threshold  $\delta_c$  after normalizing features as  $\delta_d = 2 - 2 \cdot \delta_c$ , where  $\delta_d \in [0, 4]$ . As for APIs, we follow original threshold ranges to compute optimal values.

Table 1: The FR models adopted for the robustness evaluation in this paper. \* refers to public checkpoints.

Models	Backbone	Loss	Para.(M)	Acc.(%)	Thr.
FaceNet*	InceptionResNet	Triplet	27.91	99.2	1.159
SphereFace*	Sphere20	A-Softmax	28.08	98.2	1.301
CosFace*	Sphere20	LMCL	22.67	98.7	1.507
ArcFace*	IR-SE50	Arcface	43.80	99.5	1.432
MobileFace	MobileFaceNet	LMCL	1.20	99.5	1.578
MobileNet	MobileNet	LMCL	3.75	99.4	1.683
MobileNetv2	MobileNetv2	LMCL	2.90	99.3	1.547
ShuffleNetV1	ShuffleNetV1	LMCL	1.46	99.5	1.619
ShuffleNetV2	ShuffleNetV2	LMCL	1.83	99.2	1.552
ResNet50	ResNet50	LMCL	40.29	99.7	1.618
Softmax-IR	IResNet50	Softmax	43.57	99.6	1.315
SphereFace-IR	IResNet50	A-Softmax	43.57	99.6	1.277
AM-IR	IResNet50	AM-Softmax	43.57	99.2	1.083
CosFace-IR	IResNet50	LMCL	43.57	99.7	1.552
ArcFace-IR	IResNet50	ArcFace	43.57	99.7	1.445
Microsoft API	-	-	-	98.8	0.326
Tencent API	-	-	-	99.5	51.23

**Implementation details.** We perform dodging attacks based on the pairs of images with the same identities, and impersonation attacks based on the pairs with different identities. We first use MTCNN [58] to detect facial area and align images for the entire images. Then, we obtain the cropped faces which are resized to  $112 \times 112$ . Note that the specific input size and pixel transformation will be executed inside each model due to the diversity of model inputs.

### 3.3 Evaluation Metric

Given an attack method  $\mathcal{A}_{\epsilon,p}$  that generates an adversarial example  $\mathbf{x}^{adv} = \mathcal{A}_{\epsilon,p}(\mathbf{x}, \mathbf{x}^r)$  for an input  $\mathbf{x}$  and a reference image  $\mathbf{x}^r$  with perturbation budget  $\epsilon$  under the  $\ell_p$  norm ( $\|\mathbf{x}^{adv} - \mathbf{x}\|_p \leq \epsilon$ ), the first evaluation metric is the attack success rate (Asr) on the FR model  $\mathcal{C}$  in Eq. (2), defined as

$$\text{Asr}(\mathcal{C}, \mathcal{A}_{\epsilon,p}) = \frac{1}{N} \sum_{i=1}^N \mathbb{I}(\mathcal{C}(\mathcal{A}_{\epsilon,p}(\mathbf{x}_i, \mathbf{x}_i^r), \mathbf{x}_i^r) \neq y_i), \quad (5)$$

where  $(\mathbf{x}_i, \mathbf{x}_i^r)_{i=1}^N$  is the paired test set,  $y_i$  takes 1 if the pair belongs to same identity, and 0 otherwise. The second evaluation metric is the median distance of the *minimum adversarial perturbations*, which is a metric to show the worst-case robustness of the models [1]. The objective of minimum adversarial perturbations can be denoted as

$$\min \epsilon, \text{ s.t. } \mathcal{C}(\mathcal{A}_{\epsilon,p}(\mathbf{x}_i, \mathbf{x}_i^r), \mathbf{x}_i^r) \neq y_i. \quad (6)$$

To obtain this value for each data, we perform a binary search on  $\epsilon$  to find its minimum value that fulfills the adversary’s goal.

The third evaluation metric is the *Asr vs. perturbation budget* curve, which can give a global understanding of the robustness of FR models [11]. To obtain this curve, we need to calculate Asr for all values of  $\epsilon$ , which can be efficiently done by finding the minimum perturbations and counting the number of the adversarial examples, the  $\ell_p$  norm of whose perturbations is smaller than each  $\epsilon$ . We use different criteria for different attacks, which will be specified in Sec. 4.

### 3.4 Traditional Attack Methods

To solve the problem in Eq. (3) or Eq. (4), many methods can be used to generate adversarial examples. In this section, we summarize the typical white-box and black-box adversarial attack methods that are adopted for robustness evaluations. We only introduce these methods for dodging attacks, since the extension to impersonation attacks is straightforward.

**Fast Gradient Sign Method (FGSM)** [13] generates an adversarial example given a pair of images  $\mathbf{x}$  and  $\mathbf{x}^r$  with the same identity under the  $\ell_\infty$  norm and  $\ell_2$  norm as

$$\mathbf{x}^{adv} = \mathbf{x} + \epsilon \cdot \text{sign}(\nabla_{\mathbf{x}} \mathcal{D}_f(\mathbf{x}, \mathbf{x}^r)), \quad \mathbf{x}^{adv} = \mathbf{x} + \epsilon \cdot \frac{\nabla_{\mathbf{x}} \mathcal{D}_f(\mathbf{x}, \mathbf{x}^r)}{\|\nabla_{\mathbf{x}} \mathcal{D}_f(\mathbf{x}, \mathbf{x}^r)\|_2}, \quad (7)$$

where  $\nabla_{\mathbf{x}} \mathcal{D}_f$  is the gradient of the feature distance w.r.t.  $\mathbf{x}$ , and  $\text{sign}(\cdot)$  is the sign function to make the perturbation meet the  $\ell_\infty$  norm bound.

**Basic Iterative Method (BIM)** [22] extends FGSM by iteratively taking many gradient updates as

$$\mathbf{x}_{t+1}^{adv} = \text{clip}_{\mathbf{x}, \epsilon}(\mathbf{x}_t^{adv} + \alpha \cdot \text{sign}(\nabla_{\mathbf{x}} \mathcal{D}_f(\mathbf{x}_t^{adv}, \mathbf{x}^r))), \quad (8)$$

where  $\text{clip}_{\mathbf{x}, \epsilon}$  projects the adversarial example to satisfy the  $\ell_\infty$  constrain and  $\alpha$  is the step size. We only adopt BIM for evaluations since PGD [27] and BIM result in similar attack performance.

**Momentum Iterative Method (MIM)** [8] integrates a momentum term into BIM for improving the transferability of adversarial examples as

$$\mathbf{g}_{t+1} = \mu \cdot \mathbf{g}_t + \frac{\nabla_{\mathbf{x}} \mathcal{D}_f(\mathbf{x}_t^{adv}, \mathbf{x}^r)}{\|\nabla_{\mathbf{x}} \mathcal{D}_f(\mathbf{x}_t^{adv}, \mathbf{x}^r)\|_1}; \quad \mathbf{x}_{t+1}^{adv} = \text{clip}_{\mathbf{x}, \epsilon}(\mathbf{x}_t^{adv} + \alpha \cdot \text{sign}(\mathbf{g}_{t+1})). \quad (9)$$

**Carlini & Wagner’s Method (C&W)** [2] is a powerful optimization-based attack method. It takes a Lagrangian form of the constrained optimization problem and adopts Adam [21] for optimization, which is quite effective for  $\ell_2$  attacks. However, the direct extension of the C&W method to FR is problematic since C&W uses the loss function defined on the logits of the classification models. In FR, there is not any logit output of the FR models. Thus we define a new attack objective function suitable for FR systems. For dodging attacks, the optimization problem can be formulated as

$$\mathbf{x}^{adv} = \arg \min_{\mathbf{x}'} \{ \|\mathbf{x}' - \mathbf{x}\|_2^2 + c \cdot \max(\delta - \mathcal{D}_f(\mathbf{x}', \mathbf{x}^r), 0) \}, \quad (10)$$



Figure 2: The illustration of the attention maps of the different models. We employ Grad-Gram [34] which produces the attention maps highlighting the discriminative regions.

where  $c$  is a parameter to balance the two loss terms, whose optimal value is discovered by binary search. C&W is not good at  $\ell_\infty$  attacks [2], so we only use it under the  $\ell_2$  norm.

**Transfer-based Black-box Attacks.** Under this setting, we generate adversarial examples by using the above methods against a substitute FR model, and use them to attack the black-box models. For the studied 15 FR models in our evaluations, we treat each one as the white-box model to generate adversarial examples and test the performance against the other models.

### 3.5 Landmark-Guided Cutout (LGC) Attack

Although the above attack methods can be used for attacking FR models, they are originally designed on the general image classification tasks. The adversarial examples can be highly associated with the discriminative local region of the white-box model for an input image, as emphasized in [9]. The normally trained image classification models generally have similar discriminative regions, making the crafted adversarial examples have a high transferability [9, 45]. However, we find that the existing SOTA FR models have different attention maps for their predictions given the same input image, as illustrated in Fig. 2. Therefore, the crafted adversarial examples will depend on the discriminative local region of the white-box model, making it difficult to transfer to the black-box models with different discriminative regions.

To weaken the effect of different discriminative regions for the overall transferability, we further propose a **landmark-guided cutout** (LGC) attack method. The *cutout* method [7] has been proven that it can make models take image context into consideration by randomly occluding units at the input space. Therefore, selecting appropriate occlusion from key positions can reduce sensibility of discriminative regions in the process of generating adversarial examples. Many studies have also shown that there exist some important regions for FR, including the surroundings of eyes and noses [14, 53], which are also consistent with the overall prominent regions shown in Fig. 2. Thus we extend *Cutout* to the proposed LGC method, which occludes units from *prominent* input regions of the images, making the network focus on less prominent regions and obtain more transferable adversarial examples. To achieve this goal, we apply a spatial prior by locating face landmarks by using face landmark detection [14]. Specifically, we apply a fixed-size mask to randomly sampled  $m$  locations as center points from face landmarks, and place a square patch around those locations. A simple combination of MIM and landmark-guided cutout can give rise to the LGC method as

$$\mathbf{g}_{t+1} = \mu \cdot \mathbf{g}_t + \frac{\nabla_{\mathbf{x}} \mathcal{D}_f(M_t \odot \mathbf{x}_t^{adv}, \mathbf{x}^r)}{\|\nabla_{\mathbf{x}} \mathcal{D}_f(M_t \odot \mathbf{x}_t^{adv}, \mathbf{x}^r)\|_1}; \quad \mathbf{x}_{t+1}^{adv} = \text{clip}_{\mathbf{x}, \epsilon}(\mathbf{x}_t^{adv} + \alpha \cdot \text{sign}(\mathbf{g}_{t+1})), \quad (11)$$

where  $M_t \in \{0, 1\}^d$  is a binary mask,  $\odot$  is the element-wise dot product, and  $d$  is the dimension of the face image. In the  $t$ -th iteration, after initializing the values of  $M_t$  as 1, the some randomly sampled fixed-size small square regions are set to 0 to form  $M_t$ . The algorithm is summarized in Appendix C.1. We regard the combination of LGC and MIM as **LGC attack** as default in this paper. Besides, we demonstrate that the proposed LGC can also be incorporated into other black-box attack methods to improve their performances, such as DIM [51] and TIM [9] in Appendix C.4.

### 3.6 Defense Methods

Extensive research has concentrated on building robust models against adversarial attacks on image classification. Below we introduce two general and representative categories to adapt the FR task.

**Input Transformation.** Some defenses transform the inputs before feeding them into networks, including JPEG compression [12] and bit-depth reduction [52], or add some randomness on the input [50]. We incorporate these input transformations into the natural FR models for defenses.

**Adversarial Training (AT).** AT is one of the most effective methods on defending adversarial attacks [1, 24, 57]. PGD-AT [28], as the most popular one, formulates the AT procedure as a min-max

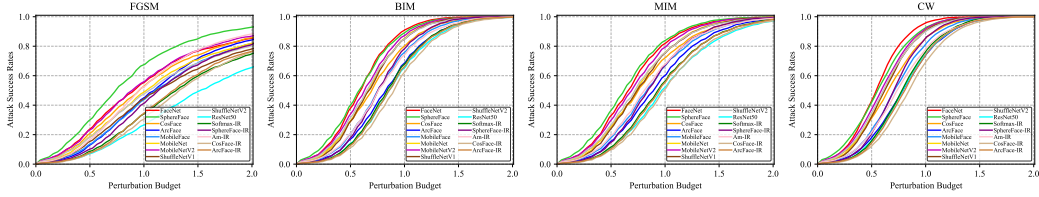


Figure 3: Asr vs. *perturbation budget* curves of the 15 models against dodging attacks under the  $\ell_2$  norm.

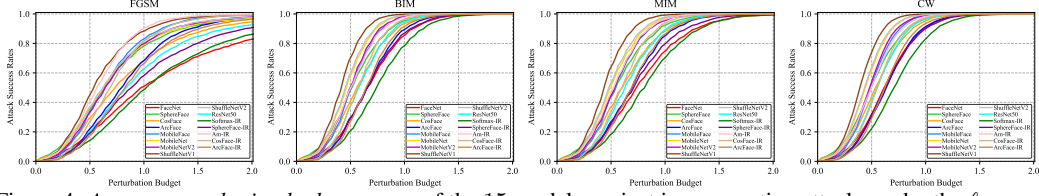


Figure 4: Asr vs. *perturbation budget* curves of the 15 models against impersonation attacks under the  $\ell_2$  norm.

problem. Therefore, AT methods in FR can be formulated as the two-stage framework:

$$\min_{\omega, \mathbf{W}} \frac{1}{n} \sum_{i=1}^n \max_{\boldsymbol{\eta}_i \in \mathcal{S}} \mathcal{L}(f(\mathbf{x}_i + \boldsymbol{\eta}_i), y_i, \mathbf{W}), \quad (12)$$

where  $f(\cdot)$  is the feature extractor with parameters  $\omega$ , the matrix  $\mathbf{W} = (W_1, \dots, W_C)$  is the weight matrix for the task with  $C$  labels,  $\mathcal{L}$  is a cross-entropy loss, and  $\mathcal{S} = \{\boldsymbol{\eta} : \|\boldsymbol{\eta}\|_\infty \leq \epsilon\}$  is a set of allowed points around  $\mathbf{x}$  with the perturbation  $\epsilon$ . Adversarial examples are crafted in the inner maximization, and model parameters are optimized by solving the outer minimization. Therefore, they are iteratively executed in training until model parameters  $\omega$  and  $\mathbf{W}$  converge. PGD [28] has been extensively applied in the inner optimization, which is denoted by taking multiple steps as

$$\boldsymbol{\eta}_i^{t+1} = \prod_{\mathcal{S}} (\boldsymbol{\eta}_i^t + \alpha \cdot \text{sign}(\nabla_{\mathbf{x}} \mathcal{L}(f(\mathbf{x} + \boldsymbol{\eta}_i^t), y_i, \mathbf{W}))), \quad (13)$$

where  $\boldsymbol{\eta}_i$  is the perturbation at the  $t$ -th step,  $\alpha$  is the step size and  $\prod(\cdot)$  is a projection function in  $\mathcal{S}$ . In this paper, we mainly consider the representative AT framework named PGD-AT [28], and adaptively integrate different loss functions (as detailed in Appendix D) into Eq. (12) with an AT procedure. Besides, another typical framework TRADES [57] is also evaluated as a comparison.

## 4 Evaluation Results

Since the input size is different for each FR model, we adopt the normalized  $\ell_2$  distance defined as  $\bar{\ell}_2(\mathbf{a}) = \|\mathbf{a}\|_2 / \sqrt{d}$  as the measurement for  $\ell_2$  attacks, where  $d$  is the dimension of a vector  $\mathbf{a}$ . We set  $\alpha = 1.5\epsilon/T$  for iterative methods, where  $T$  is the maximum step. And we set  $\mu = 1.0$  for MIM and  $c = 10^{-3}$  for C&W. For LGC, the mask consists of four squares with a side length of 7, and each square uses a randomly selected key point as the center. We compare LGC with a baseline called *cutout iterative method* (CIM) that performs random cutout in Appendix C.2, and perform ablation studies of LGC in Appendix C.3. Due to the limited space, we only present the results on LFW. The results on commercial APIs and other datasets are listed in Appendix E and Appendix F, respectively.

### 4.1 White-box Evaluation Results

We fixed the attack iterations as 20 for BIM and MIM and 100 for C&W. To get minimum perturbation, a binary search with 10 iterations is used after finding a feasible adversarial example by linear search.

**Relationship between precision and robustness.** We show the results in Fig. 3, Fig. 4, and Tab. 2. Among attacks, C&W attack gets the best performance, which accords with the performance on the general image classification [11, 39]. However, we observe that those methods with the glorious precision, e.g., ArcFace and CosFace, do not have a positive effect on robustness, which is inconsistent with the conclusion of evaluating robustness for the ImageNet classification task where there exists a trade-off between precision and robustness. Therefore, this is worth noting that learning more discriminative features from the metric space for precision cannot substantially improve robustness.

**Effects of different factors.** On the whole, model architecture is a more critical factor for robustness than loss functions. The models with a larger size of weights are more resistant to attacks under

Table 2: The median distance of the *minimum perturbations* of the 15 models against dodging and impersonation attacks under the  $\ell_2$  and  $\ell_\infty$  norms.

	$\ell_2$								$\ell_\infty$					
	FGSM		BIM		MIM		C&W		FGSM		BIM		MIM	
	dod.	imp.	dod.	imp.	dod.	imp.	dod.	imp.	dod.	imp.	dod.	imp.	dod.	imp.
FaceNet	0.92	1.17	0.59	0.66	0.66	0.73	0.54	0.61	1.75	2.14	1.17	1.31	1.28	1.42
SphereFace	0.73	0.64	0.58	0.52	0.62	0.55	0.56	0.50	1.31	1.11	1.06	0.92	1.12	0.97
CosFace	0.97	0.73	0.69	0.56	0.75	0.59	0.65	0.54	1.69	1.25	1.30	1.00	1.39	1.06
ArcFace	1.09	0.80	0.83	0.66	0.89	0.69	0.79	0.64	1.97	1.42	1.53	1.20	1.62	1.25
MobileFace	1.11	0.62	0.75	0.50	0.83	0.53	0.71	0.49	1.98	1.12	1.44	0.94	1.55	0.97
MobileNet	1.03	0.64	0.67	0.47	0.73	0.50	0.62	0.44	1.75	1.08	1.22	0.83	1.31	0.88
MobileNetV2	0.89	0.64	0.62	0.50	0.69	0.53	0.59	0.48	1.55	1.12	1.17	0.91	1.25	0.95
ShuffleNetV1	1.12	0.53	0.67	0.41	0.75	0.44	0.62	0.39	2.02	0.97	1.28	0.77	1.39	0.80
ShuffleNetV2	1.06	0.62	0.66	0.45	0.72	0.48	0.61	0.43	1.86	1.08	1.23	0.84	1.31	0.88
ResNet50	1.53	0.84	0.86	0.58	0.97	0.62	0.79	0.55	2.64	1.44	1.59	1.05	1.75	1.11
Softmax-IR	1.30	1.05	0.84	0.73	0.94	0.81	0.78	0.71	2.36	1.86	1.66	1.41	1.80	1.50
SphereFace-IR	1.14	0.90	0.77	0.66	0.84	0.70	0.70	0.63	2.12	1.62	1.50	1.25	1.62	1.31
Am-IR	0.95	0.56	0.77	0.50	0.81	0.52	0.74	0.49	1.67	1.00	1.41	0.92	1.47	0.94
CosFace-IR	1.33	0.69	0.91	0.56	0.98	0.59	0.85	0.55	2.45	1.27	1.78	1.09	1.91	1.14
ArcFace-IR	1.28	0.83	0.86	0.64	0.95	0.69	0.81	0.62	2.39	1.55	1.72	1.25	1.84	1.31

Table 3: The median distance of the *minimum perturbations* of different defense methods against dodging and impersonation attacks under the  $\ell_2$  and  $\ell_\infty$  norms.

	Clean	$\ell_2$								$\ell_\infty$					
		FGSM		BIM		MIM		C&W		FGSM		BIM		MIM	
		dod.	imp.	dod.	imp.	dod.	imp.	dod.	imp.	dod.	imp.	dod.	imp.	dod.	imp.
JPEG [12]	99.6	2.46	2.00	1.36	1.16	1.31	1.12	0.75	0.67	4.19	3.31	2.77	2.23	2.58	2.16
Bit-Red [52]	99.6	1.37	1.06	0.86	0.73	0.92	0.78	0.78	0.74	3.00	2.00	2.00	1.12	2.00	1.67
R&P [50]	99.4	4.50	8.01	2.05	2.20	2.28	2.50	1.86	2.02	8.00	10.31	4.56	4.77	4.25	4.59
PGD-AT [28]	91.3	4.14	3.95	2.37	2.37	2.70	2.70	2.06	2.14	12.94	12.38	10.34	10.23	10.83	10.62
TRADES [57]	91.0	4.37	4.41	2.70	2.73	3.03	3.03	2.38	2.51	12.69	12.12	10.59	10.30	10.97	10.64
SphereFace-AT	88.9	3.31	6.79	1.72	2.34	2.03	2.92	1.43	1.93	12.88	19.56	9.88	12.69	10.56	13.67
Am-AT	85.0	3.78	4.25	2.31	2.64	2.61	2.92	2.00	2.41	11.62	12.50	9.88	10.64	10.20	11.02
CosFace-AT	86.2	3.67	3.80	2.30	2.37	2.59	2.67	1.96	2.16	11.50	11.56	9.83	10.02	10.14	10.34
ArcFace-AT	87.7	3.43	4.55	2.16	2.61	2.39	2.95	1.86	2.35	11.62	13.81	9.89	11.42	10.19	11.84

both norms. Thus selecting a proper larger network structure as a backbone usually leads to better resistance against adversarial examples, which also provides an insight for robustness.

**Effects of different defenses.** For PGD-AT and TRADES, we set  $\epsilon = 8/255$ ,  $\alpha = 1/255$ , and the number iteration as 9 under  $\ell_\infty$  norm on CASIA-WebFace [56]. As shown in Tab. 3, AT is the most robust method, which presents consistent performance on different adaptive loss constraints. TRADES performs slightly better than PGD-AT. Their robustness can generalize to the  $\ell_2$  threat models when they are trained by the  $\ell_\infty$ . However, the overall performance against the  $\ell_2$  threat models is inferior to the  $\ell_\infty$  threat models. Besides, AT still results in a reduction of natural accuracy.

## 4.2 Black-box Evaluation Results

For black-box attacks, we fix the perturbation budget as  $\epsilon = 8$  for  $\ell_\infty$  attacks and  $\epsilon = 4$  for  $\ell_2$  attacks. Considering that black-box attacks are harder than white-box attacks, we perform 100 iterations for iterative attacks. We choose a model as the substitute model to attack the others, and we show  $Asr$  of the 15 models against dodging and impersonation attacks under the  $\ell_\infty$  norm in Fig. 5 and Fig. 6.

**Performance analysis.** We observe that the same model has a similar overall transferable trend for different attack methods. Obviously, LGC improves the transferability of adversarial examples over FGSM, BIM, and MIM, resulting in higher  $Asr$  against the black-box models. Thus landmark-guided prior knowledge is beneficial for exploring transferable adversarial examples for the FR task.

**Robustness of different models.** We observe that model architecture is a very important factor for robustness. Those models within the same architecture family have good transferability across each other. The models with light weights (e.g., MobileNet and ShuffleNet) are easily attacked by the adversarial examples generated against other models. One potential reason is that many networks (e.g., MobileNet and ShuffleNet) are based on improvements in the residual unit.

**Robustness of different optimization loss.** We find that the models among Am-IR, CosFace-IR and ArcFace have mutual transferability because their optimizations lie in angular space combined with additive margin. FaceNet is the most difficult one to transfer to other models, which is trained on InceptionResNetV1 based on the triplet loss in the Euclidean space. This might provide new valuable insights for designing robust models against black-box attacks that selecting diverse backbones and train function will restrict the transferability of adversarial samples by common white-box FR models.



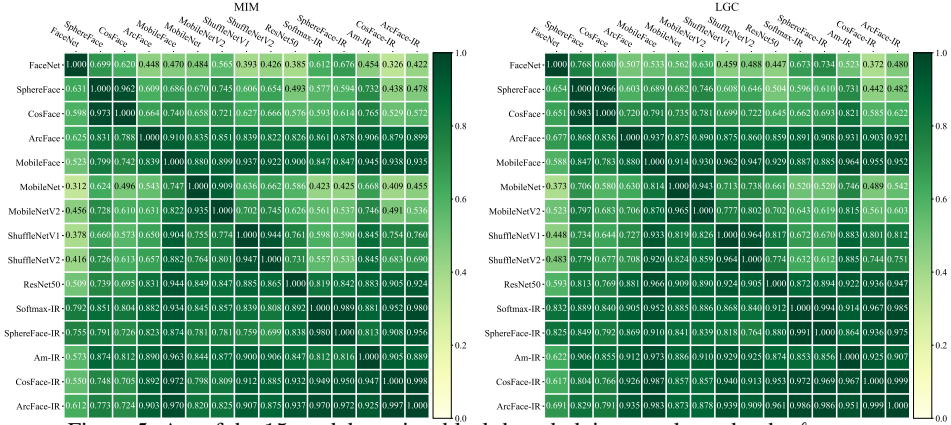


Figure 5: Asr of the 15 models against black-box dodging attacks under the  $\ell_\infty$  norm.

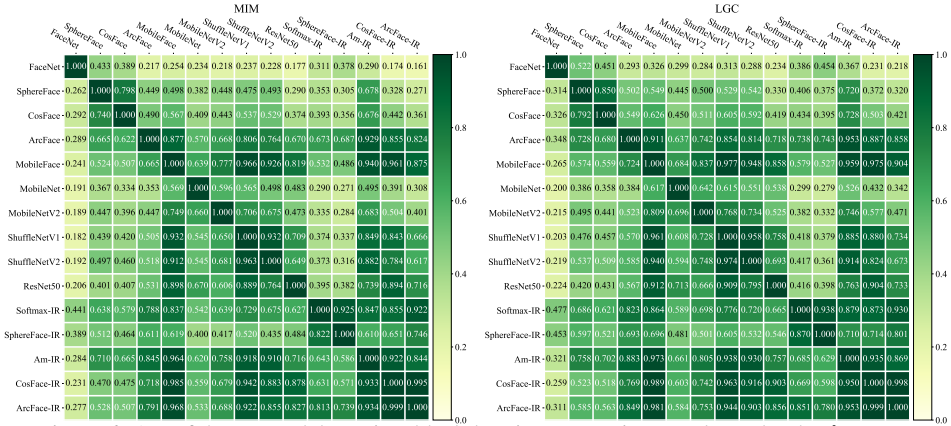


Figure 6: Asr of the 15 models against black-box impersonation attacks under the  $\ell_\infty$  norm.

### 4.3 Findings and Discussions

**First**, current mainstream models on FR, e.g., ArcFace and CosFace, have learned more discriminative features from the metric space, yet failing to substantially improve robustness. Targeted exploration of designing models is significantly taking into account robustness. **Second**, we observe model architecture is a more critical factor. Light-weight models, e.g., MobileNet and ShuffleNet, have worse defensive performance than those of normal weights under all white-box and black-box settings. Thus selecting a suitable larger network structure as a backbone seems more effective for robustness. **Third**, AT is the most robust method among the defense methods studied in this paper, which presents consistent performance on different adaptive face loss constraints. However, the robustness under the  $\ell_2$  norms is inferior to the  $\ell_\infty$  norms that are used in the training phase. Besides, AT still results in a reduction of natural accuracy and high training cost in FR. **Fourth**, we observe that the models with similar structure have higher transferability. Besides, similar training loss functions are also mutually transferable, such as LCML, ArgFace, and Am-Softmax. **Fifth**, the attack performance under  $\ell_2$  and  $\ell_\infty$  norms is very similar in generalization ability for those models belonging to the normal training. Besides, the difficulty of impersonation attacks is higher than that of dodging attacks. **Sixth**, the proposed LGC makes the generated adversarial examples more transferable based on the characteristics of face tasks, which can be flexibly applied to many black-box attack methods, such as MIM, DIM and TIM. **Seventh**, similar overall robustness conclusions across different testing datasets are presented for the same FR models, including the widely used LFW, YTF, CFP-FP and MegaFace.

## 5 Conclusion

To the best of our knowledge, we performed the largest experiment on evaluating the adversarial robustness on FR, covering diverse FR models against both white-box and black-box attacks. We conjecture that robustness should also be considered in model designs while pursuing higher accuracy. We also provide thorough evaluation metrics and valuable insights on robust FR of future works, and even in other metric learning tasks such as image retrieval, objective re-identification, and so on.

## References

- [1] Wieland Brendel, Jonas Rauber, Alexey Kurakin, Nicolas Papernot, Behar Velicq, Sharada P Mohanty, Florian Laurent, Marcel Salathé, Matthias Bethge, Yaodong Yu, et al. Adversarial vision challenge. In *The NeurIPS'18 Competition*, pages 129–153. Springer, 2020.
- [2] Nicholas Carlini and David Wagner. Towards evaluating the robustness of neural networks. In *IEEE Symposium on Security and Privacy*, 2017.
- [3] Nicholas Carlini, Anish Athalye, Nicolas Papernot, Wieland Brendel, Jonas Rauber, Dimitris Tsipras, Ian Goodfellow, and Aleksander Madry. On evaluating adversarial robustness. *arXiv preprint arXiv:1902.06705*, 2019.
- [4] Sheng Chen, Yang Liu, Xiang Gao, and Zhen Han. Mobilefacenets: Efficient cnns for accurate real-time face verification on mobile devices. In *Chinese Conference on Biometric Recognition*, pages 428–438. Springer, 2018.
- [5] Jiankang Deng, Jia Guo, Niannan Xue, and Stefanos Zafeiriou. Arcface: Additive angular margin loss for deep face recognition. In *The IEEE Conference on Computer Vision and Pattern Recognition (CVPR)*, 2019.
- [6] Jiankang Deng, Jia Guo, Niannan Xue, and Stefanos Zafeiriou. Arcface: Additive angular margin loss for deep face recognition. In *Proceedings of the IEEE Conference on Computer Vision and Pattern Recognition*, pages 4690–4699, 2019.
- [7] Terrance DeVries and Graham W Taylor. Improved regularization of convolutional neural networks with cutout. *arXiv preprint arXiv:1708.04552*, 2017.
- [8] Yinpeng Dong, Fangzhou Liao, Tianyu Pang, Hang Su, Jun Zhu, Xiaolin Hu, and Jianguo Li. Boosting adversarial attacks with momentum. In *Proceedings of the IEEE Conference on Computer Vision and Pattern Recognition (CVPR)*, 2018.
- [9] Yinpeng Dong, Tianyu Pang, Hang Su, and Jun Zhu. Evading defenses to transferable adversarial examples by translation-invariant attacks. In *Proceedings of the IEEE Conference on Computer Vision and Pattern Recognition (CVPR)*, 2019.
- [10] Yinpeng Dong, Hang Su, Baoyuan Wu, Zhifeng Li, Wei Liu, Tong Zhang, and Jun Zhu. Efficient decision-based black-box adversarial attacks on face recognition. In *Proceedings of the IEEE Conference on Computer Vision and Pattern Recognition (CVPR)*, 2019.
- [11] Yinpeng Dong, Qi-An Fu, Xiao Yang, Tianyu Pang, Hang Su, Zihao Xiao, and Jun Zhu. Benchmarking adversarial robustness on image classification. In *Proceedings of the IEEE/CVF Conference on Computer Vision and Pattern Recognition*, pages 321–331, 2020.
- [12] Gintare Karolina Dziugaite, Zoubin Ghahramani, and Daniel M Roy. A study of the effect of jpg compression on adversarial images. *arXiv preprint arXiv:1608.00853*, 2016.
- [13] Ian J Goodfellow, Jonathon Shlens, and Christian Szegedy. Explaining and harnessing adversarial examples. In *International Conference on Learning Representations (ICLR)*, 2015.
- [14] Srinivas Gutta, Vasanth Philomin, and Miroslav Trajkovic. An investigation into the use of partial-faces for face recognition. In *fgr*, pages 33–38, 2002.
- [15] Kaiming He, Xiangyu Zhang, Shaoqing Ren, and Jian Sun. Deep residual learning for image recognition. In *CVPR*, 2016.
- [16] Kaiming He, Xiangyu Zhang, Shaoqing Ren, and Jian Sun. Identity mappings in deep residual networks. In *European Conference on Computer Vision (ECCV)*, pages 630–645. Springer, 2016.
- [17] Andrew G Howard, Menglong Zhu, Bo Chen, Dmitry Kalenichenko, Weijun Wang, Tobias Weyand, Marco Andreetto, and Hartwig Adam. Mobilenets: Efficient convolutional neural networks for mobile vision applications. *arXiv preprint arXiv:1704.04861*, 2017.
- [18] Guosheng Hu, Yongxin Yang, Dong Yi, Josef Kittler, William Christmas, Stan Z Li, and Timothy Hospedales. When face recognition meets with deep learning: an evaluation of convolutional neural networks for face recognition. In *Proceedings of the IEEE international conference on computer vision workshops*, pages 142–150, 2015.
- [19] Gary B Huang, Marwan Mattar, Tamara Berg, and Eric Learned-Miller. Labeled faces in the wild: A database for studying face recognition in unconstrained environments. In *Technical report*, 2007.

- [20] Ira Kemelmacher-Shlizerman, Steven M Seitz, Daniel Miller, and Evan Brossard. The megaface benchmark: 1 million faces for recognition at scale. In *Proceedings of the IEEE conference on computer vision and pattern recognition*, pages 4873–4882, 2016.
- [21] Diederik Kingma and Jimmy Ba. Adam: A method for stochastic optimization. In *International Conference on Learning Representations (ICLR)*, 2015.
- [22] Alexey Kurakin, Ian Goodfellow, and Samy Bengio. Adversarial examples in the physical world. In *International Conference on Learning Representations (ICLR) Workshops*, 2017.
- [23] Alexey Kurakin, Ian Goodfellow, and Samy Bengio. Adversarial machine learning at scale. In *International Conference on Learning Representations (ICLR)*, 2017.
- [24] Alexey Kurakin, Ian Goodfellow, Samy Bengio, Yinpeng Dong, Fangzhou Liao, Ming Liang, Tianyu Pang, Jun Zhu, Xiaolin Hu, Cihang Xie, et al. Adversarial attacks and defences competition. *arXiv preprint arXiv:1804.00097*, 2018.
- [25] Weiyang Liu, Yandong Wen, Zhiding Yu, Ming Li, Bhiksha Raj, and Le Song. Sphreface: Deep hypersphere embedding for face recognition. In *CVPR*, 2017.
- [26] Ningning Ma, Xiangyu Zhang, Hai-Tao Zheng, and Jian Sun. Shufflenet v2: Practical guidelines for efficient cnn architecture design. In *Proceedings of the European Conference on Computer Vision (ECCV)*, pages 116–131, 2018.
- [27] Aleksander Madry, Aleksandar Makelov, Ludwig Schmidt, Dimitris Tsipras, and Adrian Vladu. Towards deep learning models resistant to adversarial attacks. In *International Conference on Learning Representations (ICLR)*, 2018.
- [28] Aleksander Madry, Aleksandar Makelov, Ludwig Schmidt, Dimitris Tsipras, and Adrian Vladu. Towards deep learning models resistant to adversarial attacks. In *International Conference on Learning Representations (ICLR)*, 2018.
- [29] Nicolas Papernot, Fartash Faghri, Nicholas Carlini, Ian Goodfellow, Reuben Feinman, Alexey Kurakin, Cihang Xie, Yash Sharma, Tom Brown, Aurko Roy, et al. Technical report on the cleverhans v2. 1.0 adversarial examples library. *arXiv preprint arXiv:1610.00768*, 2016.
- [30] Nicolas Papernot, Patrick McDaniel, Ian Goodfellow, Somesh Jha, Z Berkay Celik, and Ananthram Swami. Practical black-box attacks against deep learning systems using adversarial examples. *arXiv preprint arXiv:1602.02697*, 2016.
- [31] Jonas Rauber, Wieland Brendel, and Matthias Bethge. Foolbox v0. 8.0: A python toolbox to benchmark the robustness of machine learning models. *arXiv preprint arXiv:1707.04131*, 2017.
- [32] Mark Sandler, Andrew Howard, Menglong Zhu, Andrey Zhmoginov, and Liang-Chieh Chen. Mobilenetv2: Inverted residuals and linear bottlenecks. In *Proceedings of the IEEE Conference on Computer Vision and Pattern Recognition*, pages 4510–4520, 2018.
- [33] Florian Schroff, Dmitry Kalenichenko, and James Philbin. Facenet: A unified embedding for face recognition and clustering. In *CVPR*, 2015.
- [34] Ramprasaath R Selvaraju, Michael Cogswell, Abhishek Das, Ramakrishna Vedantam, Devi Parikh, and Dhruv Batra. Grad-cam: Visual explanations from deep networks via gradient-based localization. In *Proceedings of the IEEE international conference on computer vision*, pages 618–626, 2017.
- [35] Soumyadip Sengupta, Jun Cheng Chen, Carlos Castillo, Vishal M. Patel, Rama Chellappa, and David W. Jacobs. Frontal to profile face verification in the wild. In *2016 IEEE Winter Conference on Applications of Computer Vision (WACV)*, 2016.
- [36] Mahmood Sharif, Sruti Bhagavatula, Lujo Bauer, and Michael K Reiter. Accessorize to a crime: Real and stealthy attacks on state-of-the-art face recognition. In *Proceedings of the 2016 ACM SIGSAC Conference on Computer and Communications Security*, pages 1528–1540. ACM, 2016.
- [37] Mahmood Sharif, Sruti Bhagavatula, and Bauer. Adversarial generative nets: Neural network attacks on state-of-the-art face recognition. *arXiv preprint arXiv:1801.00349*, 2017.
- [38] Karen Simonyan and Andrew Zisserman. Very deep convolutional networks for large-scale image recognition. In *International Conference on Learning Representations (ICLR)*, 2015.

- [39] Dong Su, Huan Zhang, Hongge Chen, Jinfeng Yi, Pin-Yu Chen, and Yupeng Gao. Is robustness the cost of accuracy?—a comprehensive study on the robustness of 18 deep image classification models. In *Proceedings of the European Conference on Computer Vision (ECCV)*, pages 631–648, 2018.
- [40] Yi Sun, Yuheng Chen, Xiaogang Wang, and Xiaoou Tang. Deep learning face representation by joint identification-verification. In *Advances in neural information processing systems*, pages 1988–1996, 2014.
- [41] Christian Szegedy, Wojciech Zaremba, Ilya Sutskever, Joan Bruna, Dumitru Erhan, Ian Goodfellow, and Rob Fergus. Intriguing properties of neural networks. In *International Conference on Learning Representations (ICLR)*, 2014.
- [42] Christian Szegedy, Wei Liu, Yangqing Jia, Pierre Sermanet, Scott Reed, Dragomir Anguelov, Dumitru Erhan, Vincent Vanhoucke, and Andrew Rabinovich. Going deeper with convolutions. In *CVPR*, 2015.
- [43] Yaniv Taigman, Ming Yang, Marc’Aurelio Ranzato, and Lior Wolf. Deepface: Closing the gap to human-level performance in face verification. In *CVPR*, 2014.
- [44] Liang Tong, Zhengzhang Chen, Jingchao Ni, Wei Cheng, Dongjin Song, Haifeng Chen, and Yevgeniy Vorobeychik. Facesec: A fine-grained robustness evaluation framework for face recognition systems. In *Proceedings of the IEEE/CVF Conference on Computer Vision and Pattern Recognition*, pages 13254–13263, 2021.
- [45] Dimitris Tsipras, Shibani Santurkar, Logan Engstrom, Alexander Turner, and Aleksander Madry. Robustness may be at odds with accuracy. *arXiv preprint arXiv:1805.12152*, 2018.
- [46] Feng Wang, Jian Cheng, Weiyang Liu, and Haijun Liu. Additive margin softmax for face verification. *IEEE Signal Processing Letters*, 25(7):926–930, 2018.
- [47] Hao Wang, Yitong Wang, Zheng Zhou, Xing Ji, Zhifeng Li, Dihong Gong, Jingchao Zhou, and Wei Liu. Cosface: Large margin cosine loss for deep face recognition. In *CVPR*, 2018.
- [48] Yandong Wen, Kaipeng Zhang, Zhifeng Li, and Yu Qiao. A discriminative feature learning approach for deep face recognition. In *ECCV*, 2016.
- [49] Lior Wolf, Tal Hassner, and Itay Maoz. Face recognition in unconstrained videos with matched background similarity. In *The IEEE Conference on Computer Vision and Pattern Recognition (CVPR)*, 2011.
- [50] Cihang Xie, Jianyu Wang, Zhishuai Zhang, Zhou Ren, and Alan Yuille. Mitigating adversarial effects through randomization. In *International Conference on Learning Representations (ICLR)*, 2018.
- [51] Cihang Xie, Zhishuai Zhang, Yuyin Zhou, Song Bai, Jianyu Wang, Zhou Ren, and Alan L Yuille. Improving transferability of adversarial examples with input diversity. In *Proceedings of the IEEE Conference on Computer Vision and Pattern Recognition (CVPR)*, 2019.
- [52] Weilin Xu, David Evans, and Yanjun Qi. Feature squeezing: Detecting adversarial examples in deep neural networks. In *Proceedings of the Network and Distributed System Security Symposium (NDSS)*, 2018.
- [53] Xiao Yang, Wenhan Luo, Linchao Bao, Yuan Gao, Dihong Gong, Shibao Zheng, Zhifeng Li, and Wei Liu. Face anti-spoofing: Model matters, so does data. In *Proceedings of the IEEE Conference on Computer Vision and Pattern Recognition*, pages 3507–3516, 2019.
- [54] Xiao Yang, Fangyun Wei, Hongyang Zhang, and Jun Zhu. Design and interpretation of universal adversarial patches in face detection. In *Computer Vision—ECCV 2020: 16th European Conference, Glasgow, UK, August 23–28, 2020, Proceedings, Part XVII 16*, pages 174–191. Springer, 2020.
- [55] Xiao Yang, Yinpeng Dong, Tianyu Pang, Hang Su, and Jun Zhu. Boosting transferability of targeted adversarial examples via hierarchical generative networks. *arXiv preprint arXiv:2107.01809*, 2021.
- [56] Dong Yi, Zhen Lei, Shengcai Liao, and Stan Z Li. Learning face representation from scratch. *arXiv preprint arXiv:1411.7923*, 2014.
- [57] Hongyang Zhang, Yaodong Yu, Jiantao Jiao, Eric P Xing, Laurent El Ghaoui, and Michael I Jordan. Theoretically principled trade-off between robustness and accuracy. In *International Conference on Machine Learning (ICML)*, 2019.
- [58] Kaipeng Zhang, Zhanpeng Zhang, Zhifeng Li, and Yu Qiao. Joint face detection and alignment using multitask cascaded convolutional networks. *IEEE Signal Processing Letters*, 23(10):1499–1503, 2016.

- [59] Xiangyu Zhang, Xinyu Zhou, Mengxiao Lin, and Jian Sun. Shufflenet: An extremely efficient convolutional neural network for mobile devices. In *Proceedings of the IEEE Conference on Computer Vision and Pattern Recognition*, pages 6848–6856, 2018.
- [60] Tianyue Zheng and Weihong Deng. Cross-pose lfw: A database for studying cross-pose face recognition in unconstrained environments. *Beijing University of Posts and Telecommunications, Tech. Rep, 5*, 2018.
- [61] Tianyue Zheng, Weihong Deng, and Jiani Hu. Cross-age lfw: A database for studying cross-age face recognition in unconstrained environments. *arXiv preprint arXiv:1708.08197*, 2017.

## A Related Adversarial Robustness Platforms

The mainstream libraries for adversarial machine learning include CleverHans [29], Foolbox [31] and RealSafe [11], which focus on image classification. These libraries or platforms cannot support our evaluations in FR in terms of attacks, defenses and evaluations. Therefore, we define the modified attack formulations and representative defenses in FR, to implement the robustness evaluation. Another related work to ours is FACESEC [44]), Specifically, FACESEC focuses on  $\ell_0$ -norm attacks involving sticker attacks against 5 naturally FR models. As a comparison, our work has differences in two main aspects: 1) we aim to perform a comprehensive robustness evaluation in FR to facilitate a better understanding of the adversarial vulnerability. Thus we try our best to involve more diverse FR models, including 15 popular *naturally trained* FR models, 9 models with representative *defense mechanisms* and 2 commercial API services; 2) FACESEC adopts adversarial patch attacks under  $\ell_0$ -norm constraint, the demos of which in the physical world are very convenient. However, adversarial patch attacks are easily affected by the position, shape and scale of the adversarial patch for different individual data points, thereby hard to guarantee the fairness and effectiveness when making a general robustness evaluation based on *large-scale* facial images with various pose, expression, and illuminations. We mainly consider more popular  $\ell_2$  and  $\ell_\infty$  threat models than  $\ell_0$ -norm ones, which are appropriate and widely applied in the robustness evaluation works [29, 31, 11]. To the best of our knowledge, we perform the *largest* experiment on evaluating the adversarial robustness on face recognition, and present many key findings and valuable insights in multiple dimensions.

## B Background

In this section, we overview the research efforts on loss functions, network architectures and different datasets in FR.

### B.1 Loss Function on FR

**Euclidean-distance-based loss.** Softmax loss is commonly adopted in image classification which encourages the separability of features. However, FR requires more discriminative features that intra-variations are larger than inter-differences. Owing to the development of deep CNNs, FR has obtained remarkable progress recently. DeepFace [43] and DeepID [40] regard FR as a multi-class classification task and train deep CNNs supervised by the softmax loss. The evolved methods [40, 33, 48] treat FR as a metric learning problem and learn highly discriminative features by Euclidean-distance-based loss. The contrastive loss [40] and triplet loss [33] are proposed to increase the Euclidean margin in the feature space between different classes. Center loss [48] aims to reduce intra-variance by assigning a learned center for each class.

**Angular-margin-based loss.** With the advanced training techniques, angular-margin-based loss [25, 47, 5] is proposed to achieve the separability among features with a larger angular distance. SphereFace [25] first introduces the angular softmax loss (A-Softmax). To overcome the optimization difficulty of A-Softmax that introduces the angular margin in a multiplicative manner, CosFace [47], AM-Softmax [46] and ArcFace [5] adopt the additive angular margin loss to improve the margin in the angular space for achieving good performance, which are easy to implement and converge without many tricky hyperparameters.

### B.2 Network Architecture on FR

**Mainstream architectures.** As advanced network architectures of image classification are constantly improved, the networks in FR are also developing gradually. The typical CNN architectures, including

VGGNet [38], GoogleNet [42] and ResNet [15], are widely introduced as the baselines in FR after directly employed or slightly modified. DeepFace [43] adopts CNNs with several locally connected layers, and FaceNet [33] achieves good performance on LFW by using a triplet loss function based on GoogleNet architecture. SphereFace [25] proposed a modified ResNet architecture to boost the adaptiveness in FR.

**Light-weight networks.** Deep CNNs with plenty of layers and millions of parameters can achieve good accuracy, yet requiring large computing resource and training cost. To tackle this problem, MobileFace [4] introduces downsampling and bottleneck residual block, achieving acceptable performance on the LFW dataset. Besides, some other light-weight CNNs in image classification, including MobileNet [17, 32] and ShuffleNet [59, 26], pay more attention on the adaptiveness and effectiveness in FR.

### B.3 Datasets

The Labeled Face in the Wild (**LFW**) dataset is the most widely used benchmark for face verification on images, which contains 13, 233 face images from 5, 749 different individuals. LFW includes faces with various pose, expression, and illuminations. The *unrestricted with labeled outside data* protocol includes 6, 000 face pairs, including 3, 000 pairs with the same identities and 3, 000 pairs with different identities. YouTube Faces Database (**YTF**) includes 3, 424 videos from 1, 595 different people. All of the video sequences are from Youtube, and the average length of a video clip of YTF is about 181 frames. The unrestricted with labeled outside data protocol contains 5, 000 video pairs, half of which belong to the same identities and the others come from different identities. Recent datasets **CPLFW** [60] and **CALFW** [61] extend LFW from the perspective of large-pose and large-age types, respectively. And **CFP-FP** [35] isolates pose variation with extreme poses like profile, where many features are occluded. The dataset contains 10 frontal and 4 profile images of 500 individuals. Similar to LFW, the standard data protocol has defined 10 splits, and contains 350 pairs with the same identities and 350 pairs with different identities. **MegaFace** [20] is a challenging dataset recently released for large-scale FR, which includes 1M images of 690K different individuals for evaluation.

## C LGC Attack

### C.1 More details about LGC

LGC occludes units from *prominent* input regions of the images, making the network focus on less prominent regions and obtain more transferable adversarial examples. To achieve this goal, we apply a spatial prior by locating face landmarks by using face landmark detection [14], as illustrated in Fig. 7. Specifically, we apply a fixed-size mask to randomly sampled  $m$  locations as center points from face landmarks, and place a square patch around those locations. A simple combination of MIM and landmark-guided cutout can give rise to the landmark-guided cutout iterative method as

$$\mathbf{g}_{t+1} = \mu \cdot \mathbf{g}_t + \frac{\nabla_{\mathbf{x}} \mathcal{D}_f(M_t \odot \mathbf{x}_t^{adv}, \mathbf{x}^r)}{\|\nabla_{\mathbf{x}} \mathcal{D}_f(M_t \odot \mathbf{x}_t^{adv}, \mathbf{x}^r)\|_1}; \quad \mathbf{x}_{t+1}^{adv} = \text{clip}_{\mathbf{x}, \epsilon}(\mathbf{x}_t^{adv} + \alpha \cdot \text{sign}(\mathbf{g}_{t+1})). \quad (14)$$

where  $M_t \in \{0, 1\}^d$  is a binary mask,  $\odot$  is the element-wise dot product, and  $d$  is the dimension of the face image. In the  $t$ -th iteration, after initializing the values of  $M_t$  as 1, the some randomly sampled fixed-size small square regions are set to 0 to form  $M_t$ . The algorithm is summarized in Algorithm 1.

### C.2 Comparison of CIM and LGC

We compare the performance of Cutout (CIM) and Landmark-Guided Cutout (LGC) on the LFW dataset. For CIM, we apply a default square zero-mask with a side length of 10 [7] to a random location at each iteration. As for LGC, the mask consists of four small squares, making a randomly selected key face landmark as the center. Note that we ensure that the total mask area used for CIM and LGC is equal. Fig. 8 and Fig. 9 show the success rates of the 15 models against black-box dodging and impersonation attacks based on CIM and LGC under the  $\ell_\infty$  norm. LGC achieves more performance under the dodging and impersonation setting. The results also demonstrate that the

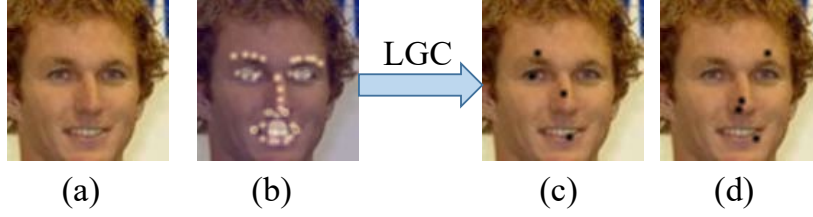


Figure 7: The illustration of the landmark-guided cutout method, where (a) is the original input, (b) has fixed number of landmarks. We randomly sample face landmarks in (b) as a mask in the process of generating adversarial examples, e.g., (c) and (d).

---

#### Algorithm 1 LGC Attack

---

**Input:** An input  $\mathbf{x}$ ; a reference image  $\mathbf{x}^r$ ; a feature representation function  $f$ ; a face landmark detection  $\mathcal{LD}$ ; the size of perturbation  $\epsilon$ ; learning rate  $\alpha$ ; iteration  $N$ ; location numbers  $m$ .

**Output:** An adversarial image.

- 1:  $\mathbf{x}_0^{adv} = \mathbf{x}$ ;  $\mathbf{g}_0 = 0$ ;  $P = \mathcal{LD}(\mathbf{x})$ ;
  - 2: **for**  $t = 0$  **to**  $N - 1$  **do**
  - 3:   Initialize a mask  $M_t$  with  $\{1\}^d$ ;
  - 4:   Randomly sample  $m$  locations  $P_m$  from  $P$ , and place a square zero-patch on  $P_m$  to form  $M_t$ ;
  - 5:   Input  $M_t \odot \mathbf{x}_t^{adv}$  and obtain the gradient  $\nabla_{\mathbf{x}} \mathcal{D}_f(M_t \odot \mathbf{x}_t^{adv}, \mathbf{x}^r)$ ;
  - 6:   Update  $\mathbf{g}_{t+1}$  and  $\mathbf{x}_{t+1}^{adv}$  by Eq. (14).
  - 7: **end for**
- 

adversarial examples generated by LGC are less sensitive to the discriminative regions, thus fooling other black-box face recognition models.

### C.3 Different Quantities and Sizes for LGC

In this section, we discuss the impact of different quantities and sizes on LGC. We choose a model from 15 models as the substitute model to attack the others. Fig. 11 and Fig. 12 show the success rates of different models against black-box dodging and impersonation attacks under different *quantities* of black-squares for LGC. Fig. 13 and Fig. 14 show the success rates of different models against black-box dodging and impersonation attacks under different *sizes* of black-squares for LGC. The value in the  $i$ -th row and the  $j$ -th column of each heatmap matrix implies the attack success rate for the target model  $j$  on the adversarial samples generated by the source models  $i$ . We found that the best results can be achieved only with the appropriate quantities and sizes of occlusions. Too big or too small is not optimal.

### C.4 Combinations of LGC and Other Attacks

**DIM** [51] relies on a stochastic transformation function to craft adversarial examples, which can be represented as

$$\mathbf{x}_{t+1}^{adv} = \text{clip}_{\mathbf{x}, \epsilon}(\mathbf{x}_t^{adv} + \alpha \cdot \text{sign}(\nabla_{\mathbf{x}} \mathcal{D}_f(T(\mathbf{x}_t^{adv}, p), \mathbf{x}^r))), \quad (15)$$

where  $T(\mathbf{x}_t^{adv}, p)$  refers to some transformation to diversify the input with probability  $p$ . Therefore, a simple combination of LGC and DIM named **LGC-DIM** can be denoted as

$$\mathbf{x}_{t+1}^{adv} = \text{clip}_{\mathbf{x}, \epsilon}(\mathbf{x}_t^{adv} + \alpha \cdot \text{sign}(\nabla_{\mathbf{x}} \mathcal{D}_f(T(M_t \odot \mathbf{x}_t^{adv}, p), \mathbf{x}^r))), \quad (16)$$

where  $M_t \in \{0, 1\}^d$  is a binary mask and  $\odot$  is the element-wise dot product, and  $d$  is the dimension of the face image. In the  $t$ -th iteration, some randomly sampled fixed-size small square regions are set to 0 to form  $M_t$ .

**TIM** [9] integrates the translation-invariant method into BIM by convolving the gradient with the pre-defined kernel  $\mathbf{W}$  as

$$\mathbf{x}_{t+1}^{adv} = \text{clip}_{\mathbf{x}, \epsilon}(\mathbf{x}_t^{adv} + \alpha \cdot \text{sign}(\mathbf{W} * \nabla_{\mathbf{x}} \mathcal{D}_f(\mathbf{x}_t^{adv}, \mathbf{x}^r))). \quad (17)$$

Similarly, a simple combination of LGC and TIM named **LGC-TIM** can be denoted as

$$\mathbf{x}_{t+1}^{adv} = \text{clip}_{\mathbf{x}, \epsilon}(\mathbf{x}_t^{adv} + \alpha \cdot \text{sign}(\mathbf{W} * \nabla_{\mathbf{x}} \mathcal{D}_f(M_t \odot \mathbf{x}_t^{adv}, \mathbf{x}^r))). \quad (18)$$

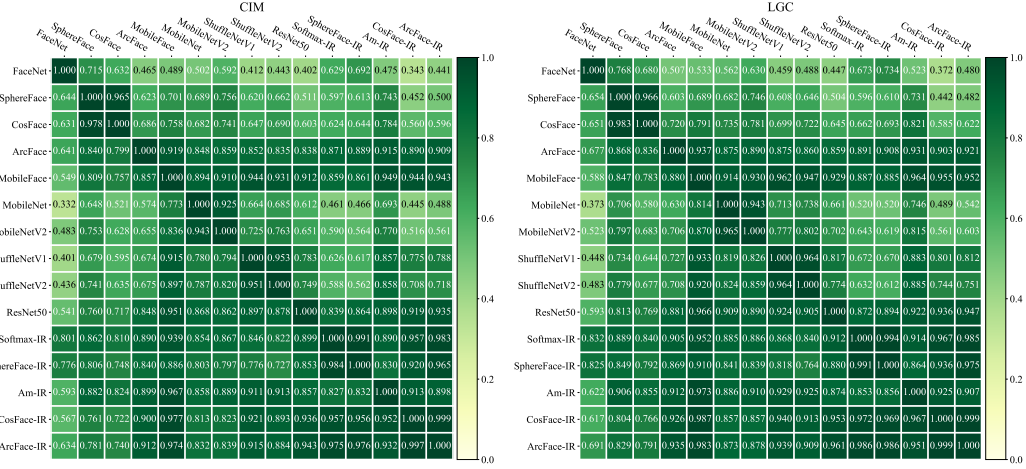


Figure 8: The success rates of the 15 models against black-box dodging attacks based on CIM and LGC under the  $\ell_\infty$  norm.

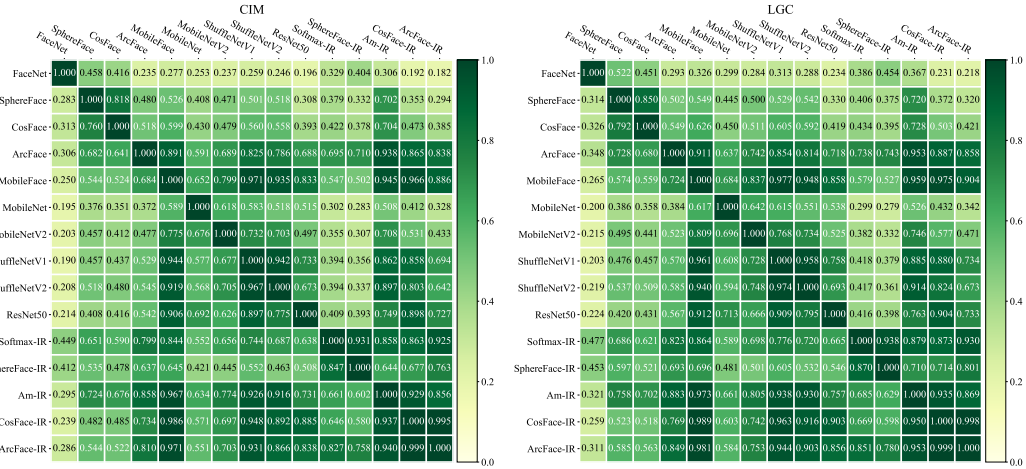


Figure 9: The success rates of the 15 models against black-box impersonation attacks based on CIM and LGC under the  $\ell_\infty$  norm.

Fig. 10 show the success rates of the 15 models against different black-box impersonation attacks based on DIM, LGC-DIM, TIM and LGC-TIM under the  $\ell_\infty$  norm. After incorporating LGC into DIM and TIM, attack algorithms achieve better performance, which also demonstrate the consistent effectiveness for the adversarial examples generated by LGC in terms of FR. Therefore, LGC can be flexibly applied to any black-box attack method to improve the performance.

## D Defense details

we mainly consider the representative AT framework named PGD-AT [28], and adaptively integrate different loss functions in Tab. 4 an AT procedure. And Fig. 16 also shows the distance distribution between normal and adversarial training.

## E Evaluation on Commercial API

We evaluate adversarial robustness on 2 commercial FR API services available at Microsoft API<sup>2</sup> and Tencent API<sup>3</sup>. The working mechanism and training data are completely unknown for us. We follow their original threshold ranges, and compute the optimal thresholds on LFW for dodging and

<sup>2</sup><https://docs.microsoft.com/>

<sup>3</sup><https://cloud.tencent.com/>



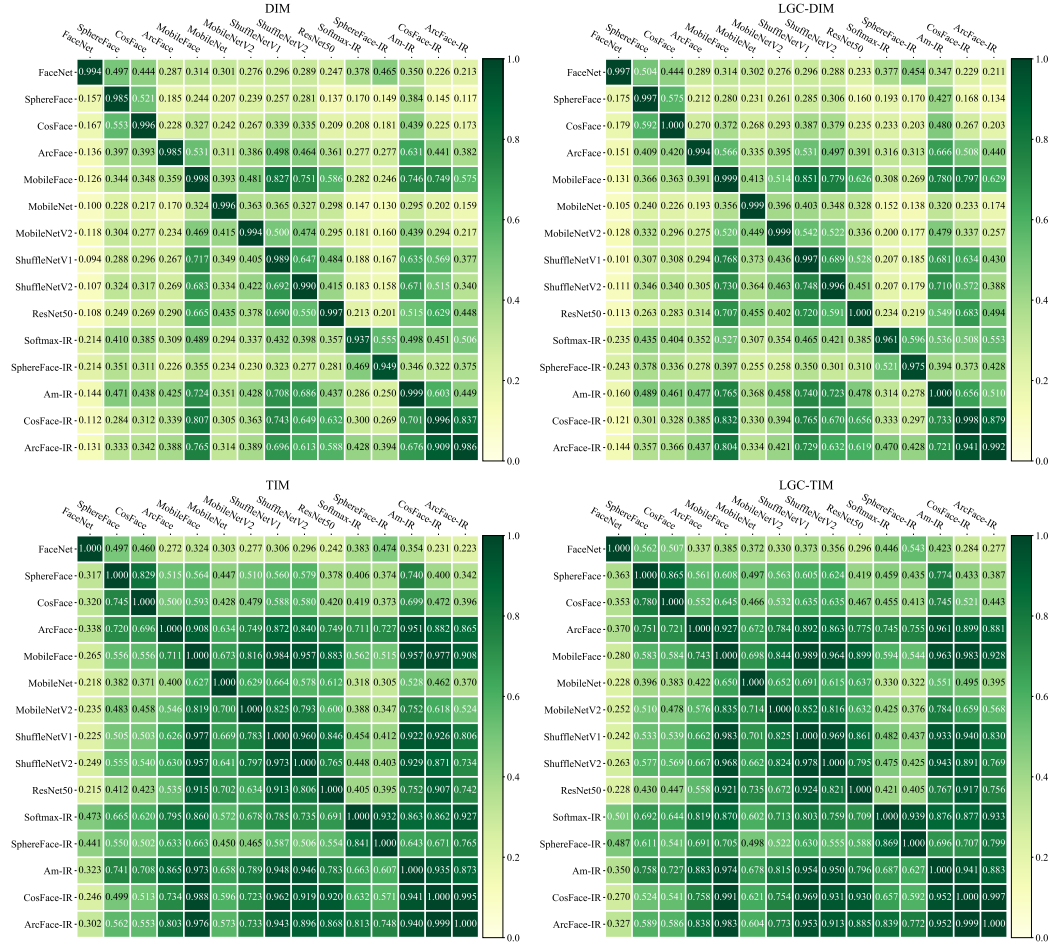


Figure 10: The success rates of the 15 models against black-box impersonation attacks under the  $\ell_\infty$  norm on LFW.

Table 4: Formulations of different loss functions  $\mathcal{L}(\mathbf{z}_i, y_i, \mathbf{W})$ .  $\mathbf{z}_i = f(\mathbf{x}_i)$  is the extracted feature vector with the input  $\mathbf{x}_i$ , and  $\theta_{i,j}$  indicates the angle between  $\mathbf{W}_i$  and  $\mathbf{z}_j$ . Note that Am-Softmax [46] and LMCL [47] possess the same formulation of loss.

Method	Loss Function $\mathcal{L}$
Softmax	$\frac{1}{N} \sum_i -\log \left( \frac{\mathbf{W}_{y_i} \cdot \mathbf{z}_i}{\sum_k e^{\mathbf{W}_k \cdot \mathbf{z}_i}} \right)$
A-Softmax [25]	$\frac{1}{N} \sum_i -\log \left( \frac{e^{\ \mathbf{W}_{y_i}\  \cdot \ \mathbf{z}_i\  \cos(m \cdot \theta_{y_i, i})}}{e^{\ \mathbf{W}_{y_i}\  \cdot \ \mathbf{z}_i\  \cos(m \cdot \theta_{y_i, i})} + \sum_{k \neq y_i} e^{\ \mathbf{W}_k\  \cdot \ \mathbf{z}_i\  \cos \theta_{k, i}}} \right)$
Am-Softmax [46]	$\frac{1}{N} \sum_i -\log \left( \frac{e^{s \cdot (\cos \theta_{y_i, i} - m)}}{e^{s \cdot (\cos \theta_{y_i, i} - m)} + \sum_{k \neq y_i} e^{s \cdot \cos \theta_{k, i}}} \right)$
LMCL [47]	$\frac{1}{N} \sum_i -\log \left( \frac{e^{s \cdot (\cos \theta_{y_i, i} - m)}}{e^{s \cdot (\cos \theta_{y_i, i} - m)} + \sum_{k \neq y_i} e^{s \cdot \cos \theta_{k, i}}} \right)$
ArcFace [5]	$\frac{1}{N} \sum_i -\log \left( \frac{e^{s \cdot \cos(\theta_{y_i, i} + m)}}{e^{s \cdot \cos(\theta_{y_i, i} + m)} + \sum_{k \neq y_i} e^{s \cdot \cos \theta_{k, i}}} \right)$

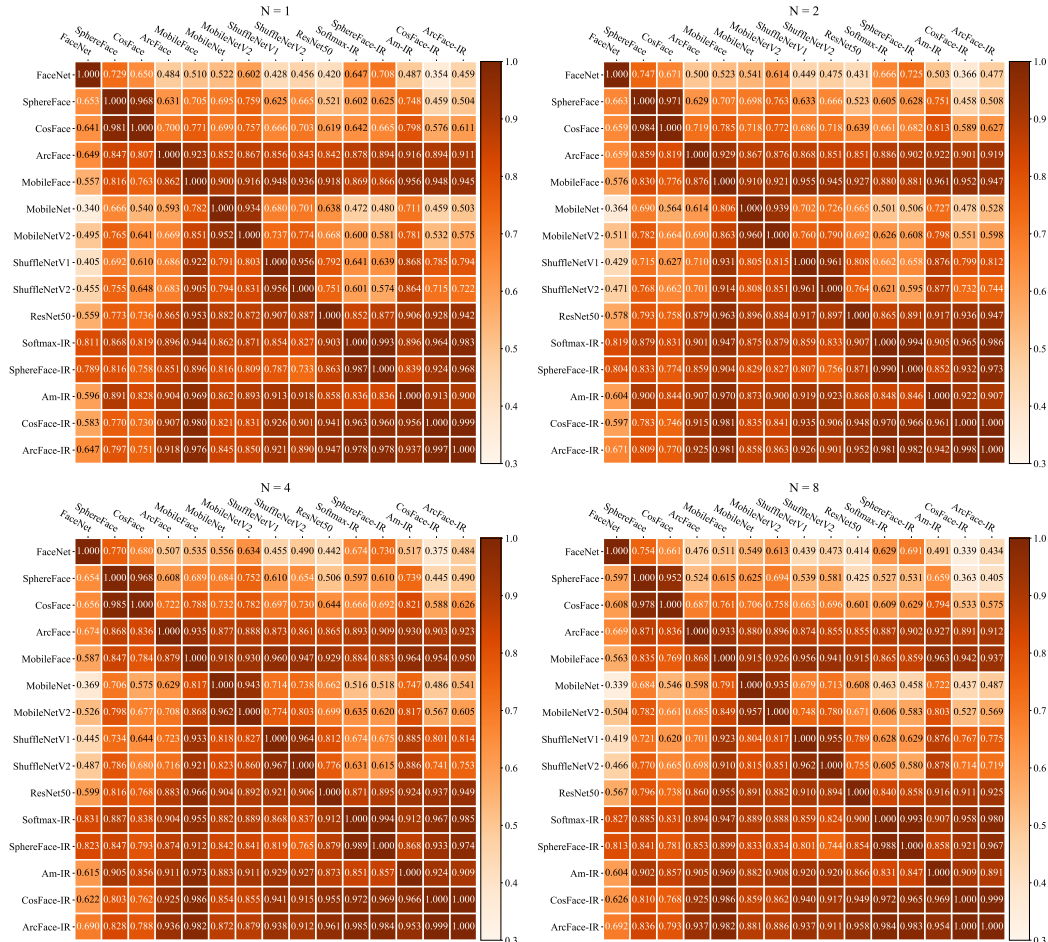


Figure 11: The success rates of the 15 models against black-box dodging attacks under different quantities of black-squares for LGC under the  $\ell_\infty$  norm on LFW.

impersonation attacks. Thus after crafting adversarial examples based on proposed LCG against ArcFace, CosFace, FaceNet and SphereFace, we then feed the generated images into black-box APIs for benchmarking adversarial robustness. Fig. 15 shows the success rates of commercial APIs against black-box dodging and impersonation attacks under the  $\ell_\infty$  norm on LFW. Microsoft API obtains unsatisfying performance on robustness with an attack success rate of 76.7% for dodging attack, 65.0% for impersonation attack. In contrast, although Tencent API presents progressive resistant performance against adversarial examples, it does not exhibit reliable effectiveness on robustness evaluation for security-critical FR systems. Thus targeted exploration of designing models is significantly taking into account robustness in the future.

## F Full Evaluation Results

In addition to the LFW dataset mentioned, we also perform an adversarial evaluation on YouTube Faces Database (YTF) [49]. Besides, experiments on larger and more challenging face verification datasets, e.g., CFP-FP [35], are shown in the following section.

### F.1 Additional results on the LFW dataset

We present the curves of FGSM, BIM, MIM under the  $\ell_\infty$  norm in Fig. 17 and Fig. 18.

### F.2 Evaluation on the YTF dataset

YTF contains 5000 video pairs, half of which belong to the same identities and others come from different identities. We select an intermediate frame as the representative image to perform our task.

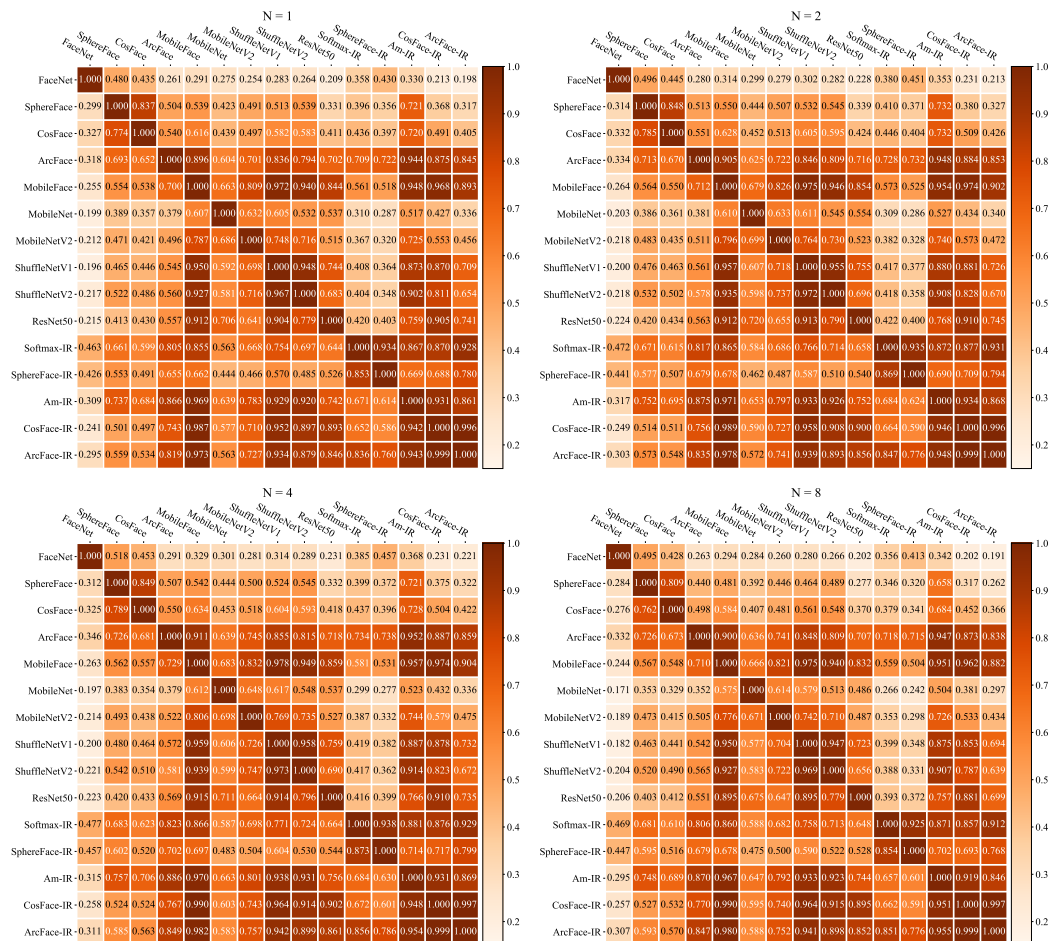


Figure 12: The success rates of the 15 models against black-box impersonation attacks under different quantities of black-squares for LGC under the  $\ell_\infty$  norm on LFW.

We perform dodging attacks based on the pairs of images with the same identities, and impersonation attacks based on the pairs with different identities. The parameter setting is the same as LFW.

**White-box attacks:** We show some robustness curves for white-box attacks and provide attack success rate vs. perturbation budget of face recognition models against dodging and impersonation attacks under the  $\ell_2$  and  $\ell_\infty$  norm. Fig. 19 and Fig. 20 show the *attack success rate vs. perturbation budget* curves of the 15 models against dodging and impersonation attacks under the  $\ell_2$  norm. Fig. 21 and Fig. 22 show the *attack success rate vs. perturbation budget* curves of the 15 models against dodging and impersonation attacks under the  $\ell_\infty$  norm.

**Transfer-based black-box attacks:** We show the attack success rate of the 15 models against dodging and impersonation attacks based on black-box FGSM, BIM, MIM, and LGC methods under the  $\ell_\infty$  norm in Fig. 23 and Fig. 24.

### E.3 Evaluation on the CFP-FP dataset

CFP-FP dataset isolates pose variation with extreme poses like profile, where many features are occluded. The dataset contains 10 frontal and 4 profile images of 500 individuals. Similar to LFW, the standard data protocol has defined 10 splits, and contains 350 pairs with the same identities and 350 pairs with different identities.

**White-box attacks:** For CFP-FP dataset, we also show some robustness curves for white-box attacks and provide attack success rate vs. perturbation budget of face recognition models against dodging and impersonation attacks under the  $\ell_2$  and  $\ell_\infty$  norm. Fig. 25 and Fig. 26 show the *attack success rate vs. perturbation budget* curves of the 15 models against dodging and impersonation attacks

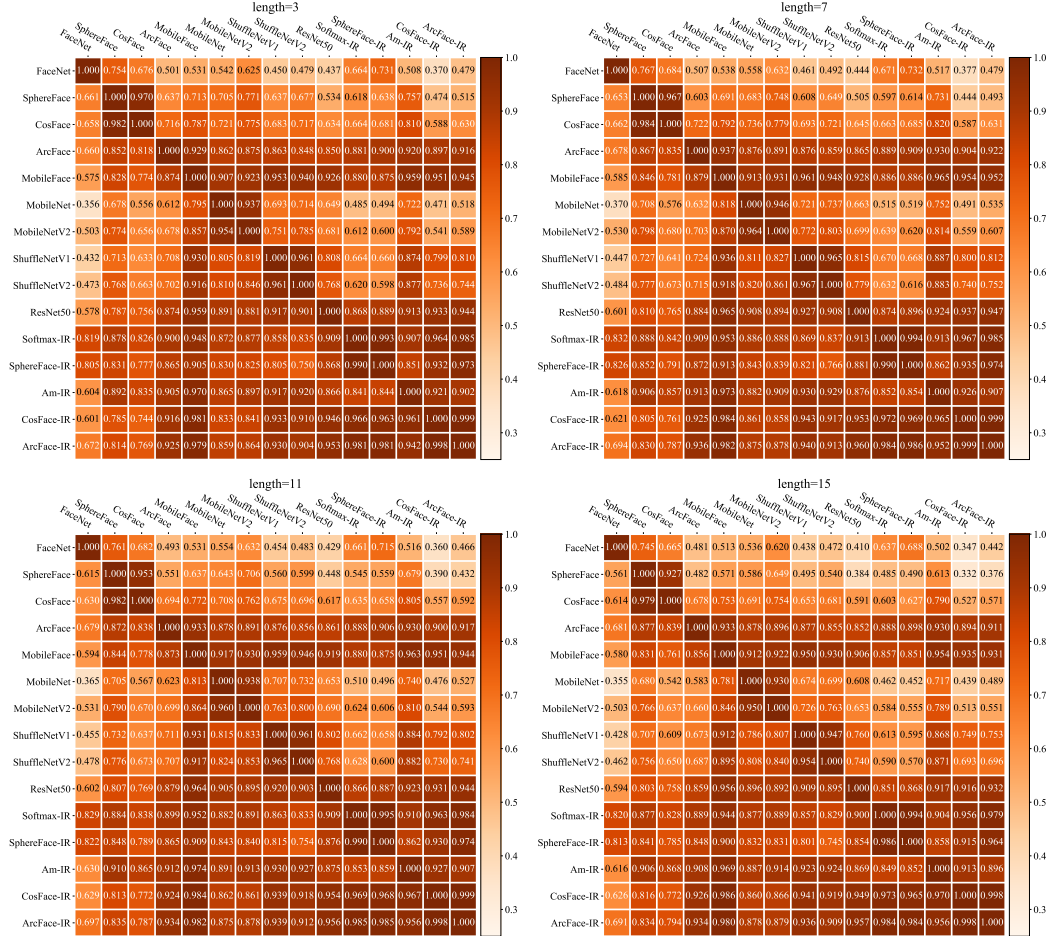


Figure 13: The success rates of the 15 models against black-box dodging attacks under different sizes of black-squares for LGC under the  $\ell_\infty$  norm on LFW.

under the  $\ell_2$  norm. Fig. 27 and Fig. 28 show the *attack success rate vs. perturbation budget* curves of the 15 models against dodging and impersonation attacks under the  $\ell_\infty$  norm.

**Transfer-based black-box attacks:** We show the attack success rate of the 15 models against dodging and impersonation attacks based on black-box FGSM, BIM, MIM, and LGC methods under the  $\ell_\infty$  norm in Fig. 29 and Fig. 30.

#### F.4 Evaluation on the MegFace dataset

MegFace isolates pose variation with extreme poses like profile, where many features are occluded. The dataset contains 10 frontal and 4 profile images of 500 individuals. Similar to LFW, the standard data protocol has defined 10 splits, and contains 350 pairs with the same identities and 350 pairs with different identities.

**White-box attacks:** For MegFace dataset, we also show some robustness curves for white-box attacks and provide attack success rate vs. perturbation budget of face recognition models against dodging and impersonation attacks under the  $\ell_2$  and  $\ell_\infty$  norm. Fig. 31 and Fig. 32 show the *attack success rate vs. perturbation budget* curves of the 15 models against dodging and impersonation attacks under the  $\ell_2$  norm. Fig. 33 and Fig. 34 show the *attack success rate vs. perturbation budget* curves of the 15 models against dodging and impersonation attacks under the  $\ell_\infty$  norm.

**Transfer-based black-box attacks:** We show the attack success rate of the 15 models against dodging and impersonation attacks based on black-box FGSM, BIM, MIM, and LGC methods under the  $\ell_\infty$  norm in Fig. 35 and Fig. 36.

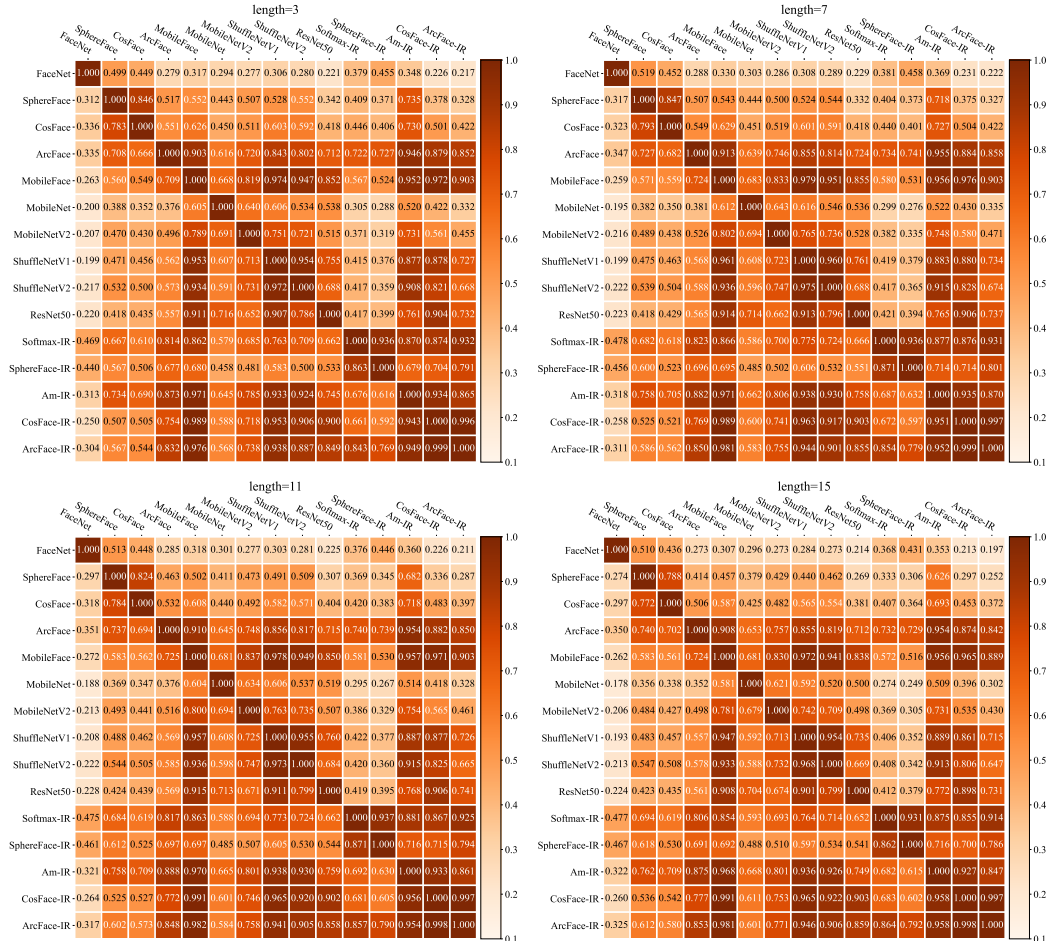


Figure 14: The success rates of the 15 models against black-box impersonation attacks under different sizes of black-squares for LGC under the  $\ell_\infty$  norm on LFW.

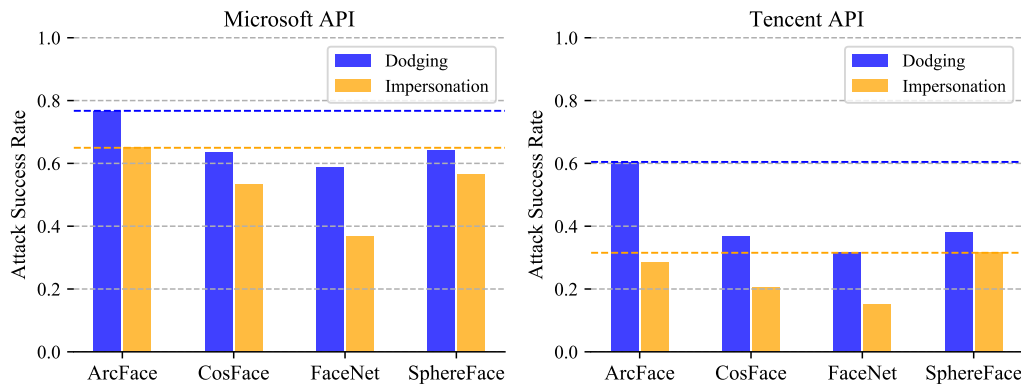


Figure 15: The success rates of commercial APIs against black-box dodging and impersonation attacks under the  $\ell_\infty$  norm on LFW.

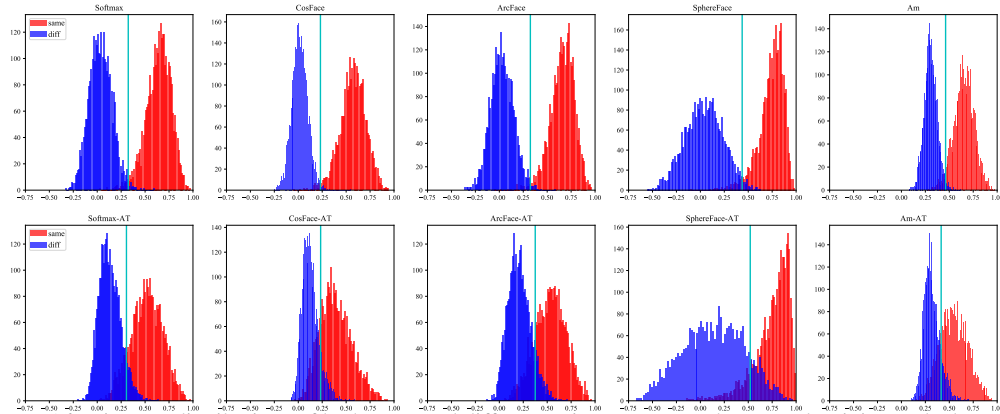


Figure 16: Distance distributions of both same and different pairs on LFW under normal training and adversarial training. The cyan lines refer to the thresholds.

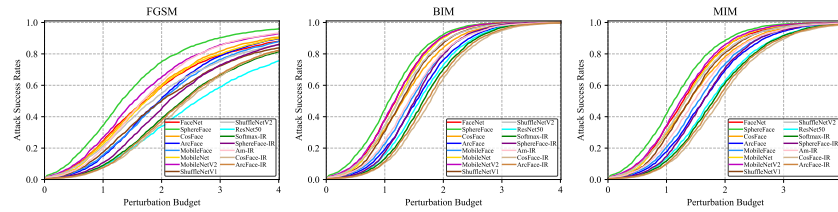


Figure 17: Asr vs. perturbation budget curves of the 15 models against dodging attacks under the  $l_\infty$  norm.

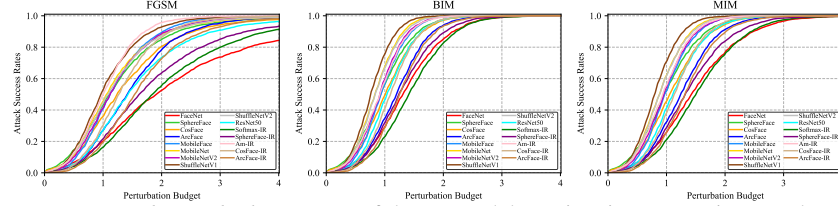


Figure 18: Asr vs. perturbation budget curves of the 15 models against impersonation attacks under the  $l_\infty$  norm.

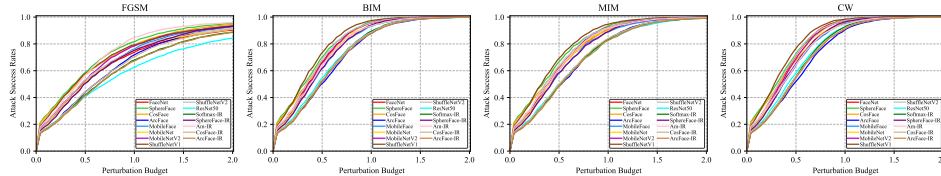


Figure 19: The attack success rate vs. perturbation budget curves of the 15 models against dodging attacks under the  $l_2$  norm on YTF.

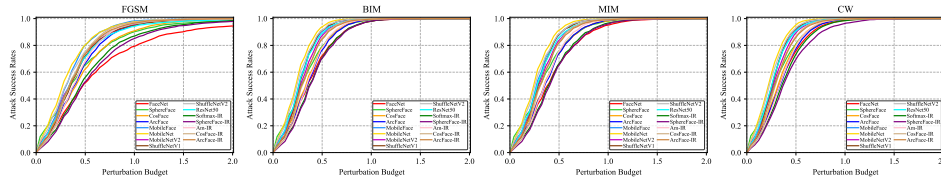


Figure 20: The attack success rate vs. perturbation budget curves of the 15 models against impersonation attacks under the  $l_2$  norm on YTF.

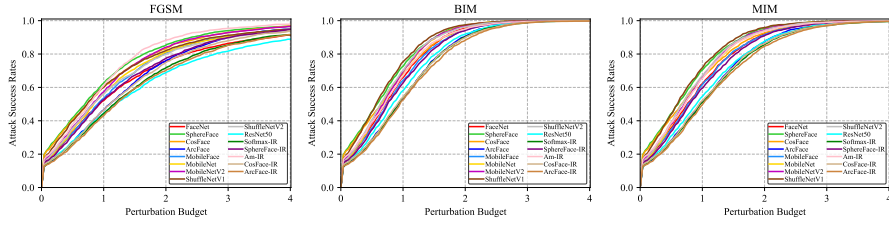


Figure 21: The attack success rate vs. perturbation budget curves of the 15 models against dodging attacks under the  $\ell_\infty$  norm on YTF.

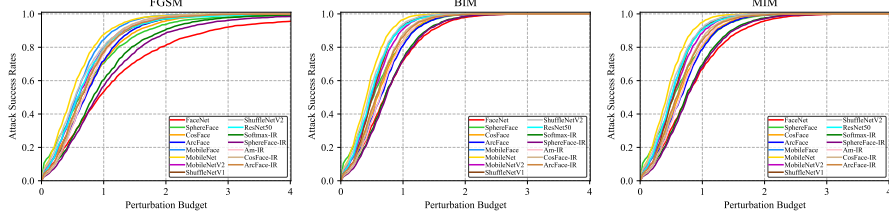


Figure 22: The attack success rate vs. perturbation budget curves of the 15 models against impersonation attacks under the  $\ell_\infty$  norm on YTF.

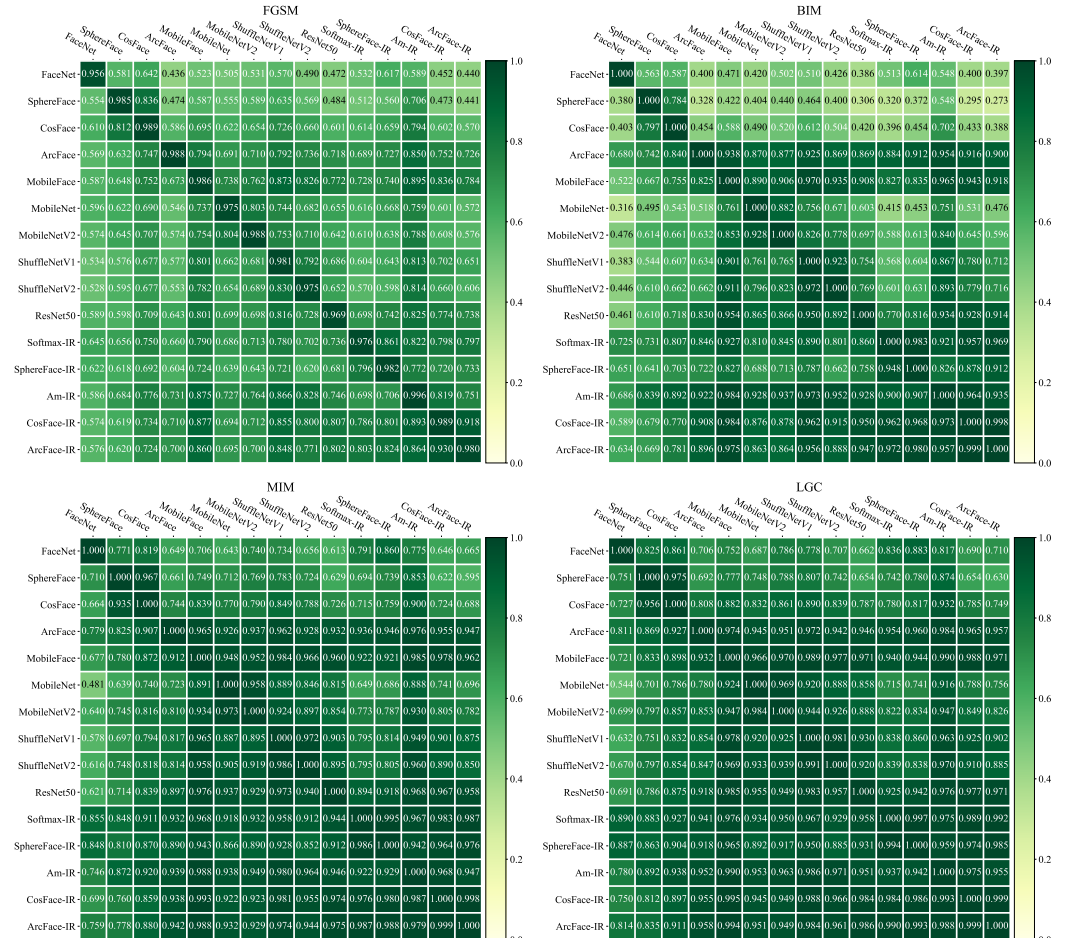


Figure 23: The success rates of the 15 models against black-box dodging attacks under the  $\ell_\infty$  norm on YTF.

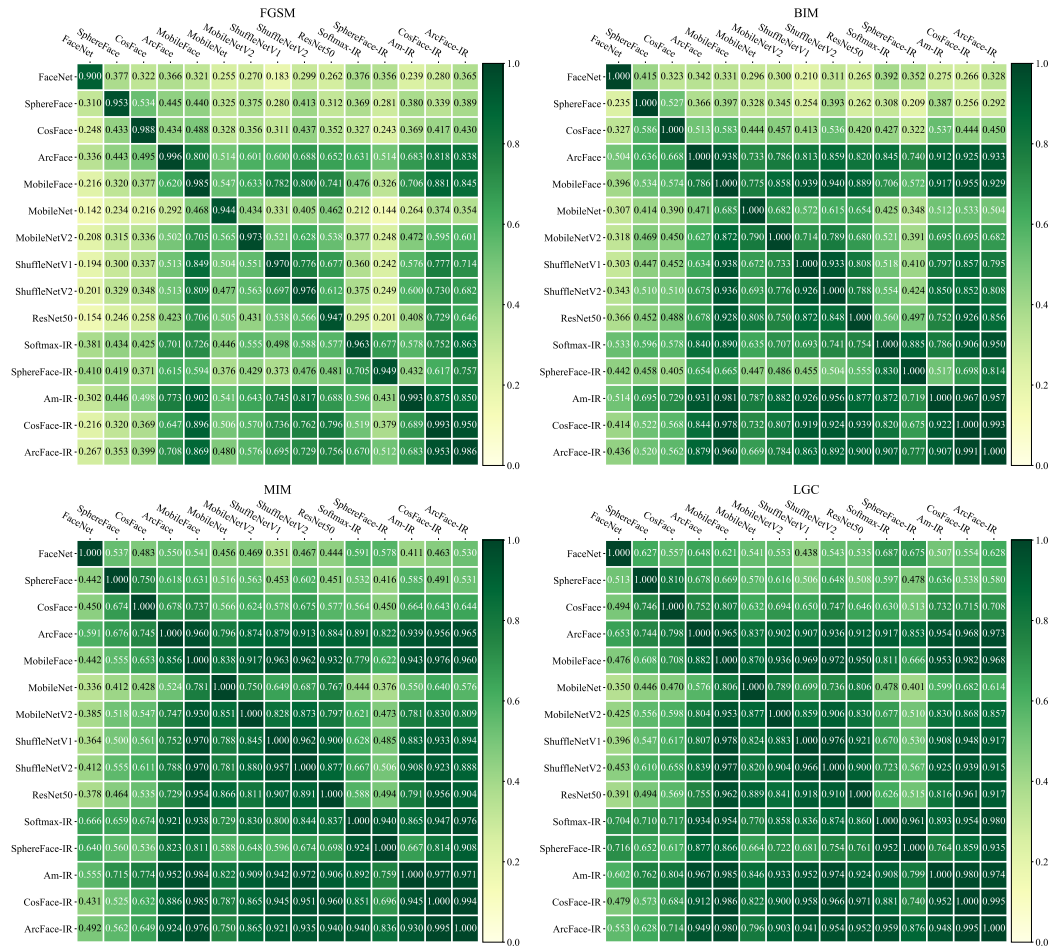


Figure 24: The success rates of the 15 models against black-box impersonation attacks under the  $\ell_\infty$  norm on YTF.

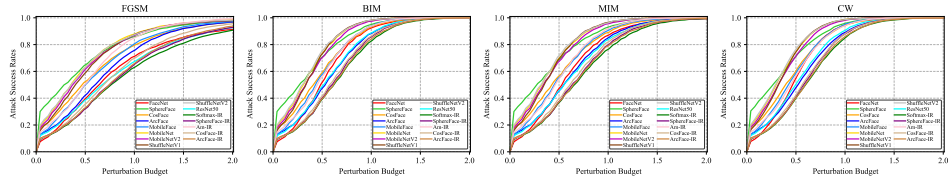


Figure 25: The attack success rate vs. perturbation budget curves of the 15 models against dodging attacks under the  $\ell_2$  norm on CFP-FP.

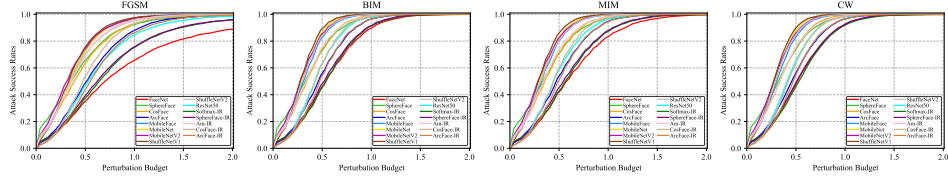


Figure 26: The attack success rate vs. perturbation budget curves of the 15 models against impersonation attacks under the  $\ell_2$  norm on CFP-FP.



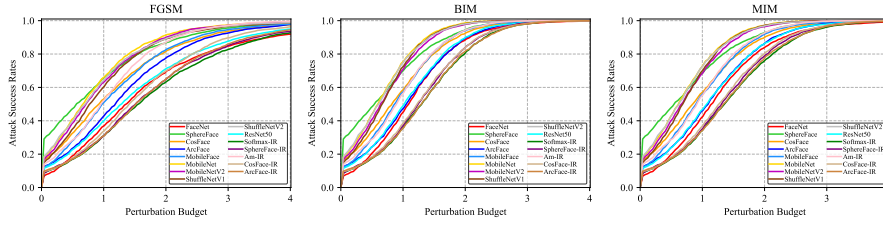


Figure 27: The attack success rate vs. perturbation budget curves of the 15 models against dodging attacks under the  $\ell_\infty$  norm on CFP-FP.

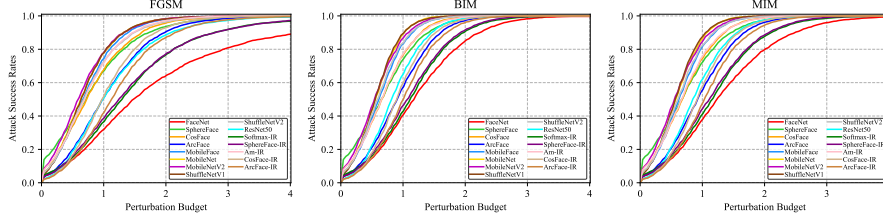


Figure 28: The attack success rate vs. perturbation budget curves of the 15 models against impersonation attacks under the  $\ell_\infty$  norm on CFP-FP.

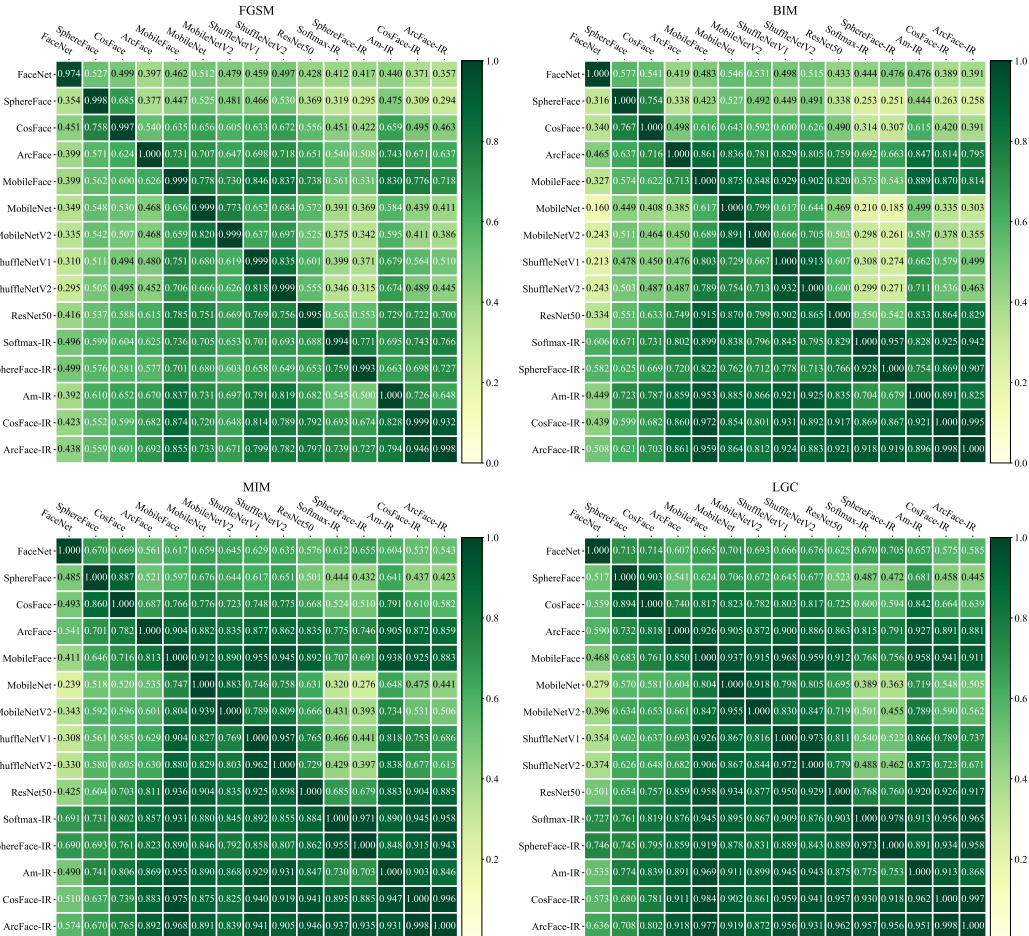


Figure 29: The success rates of the 15 models against black-box dodging attacks under the  $\ell_\infty$  norm on CFP-FP.

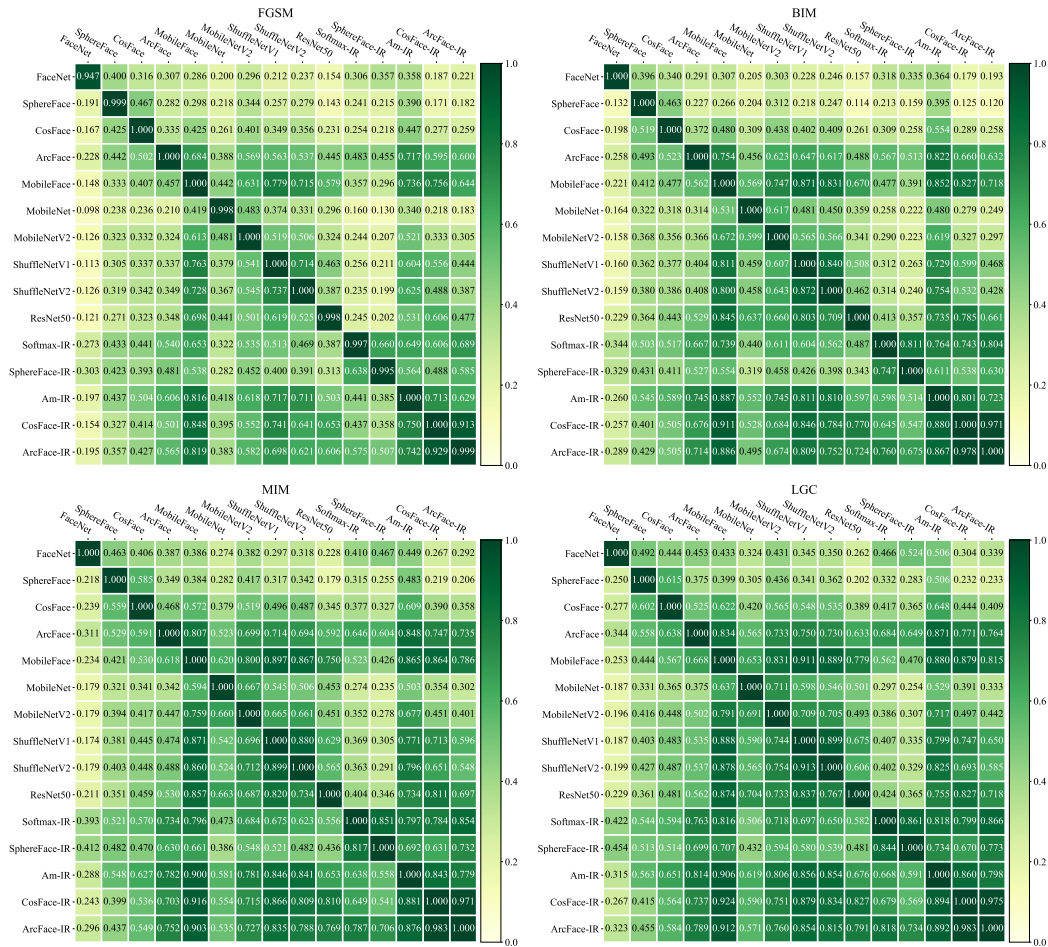


Figure 30: The success rates of the 15 models against black-box impersonation attacks under the  $\ell_\infty$  norm on CFP-FP.

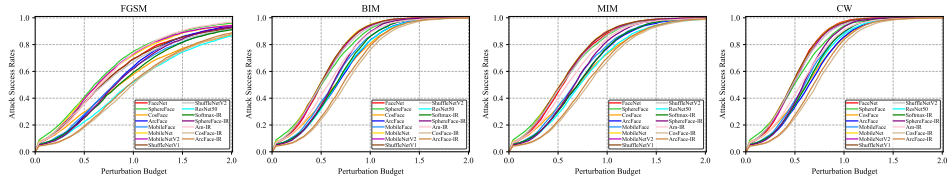


Figure 31: The attack success rate vs. perturbation budget curves of the 15 models against dodging attacks under the  $\ell_2$  norm on MegFace.

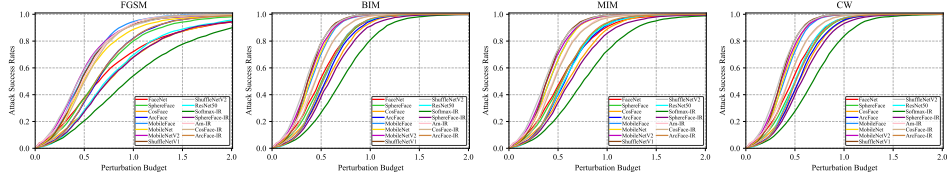


Figure 32: The attack success rate vs. perturbation budget curves of the 15 models against impersonation attacks under the  $\ell_2$  norm on MegFace.

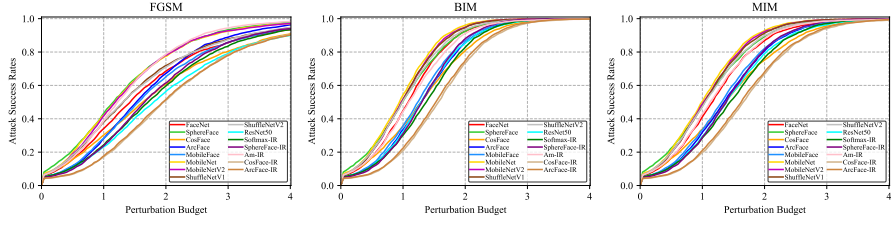


Figure 33: The attack success rate vs. perturbation budget curves of the 15 models against dodging attacks under the  $\ell_\infty$  norm on MegFace.

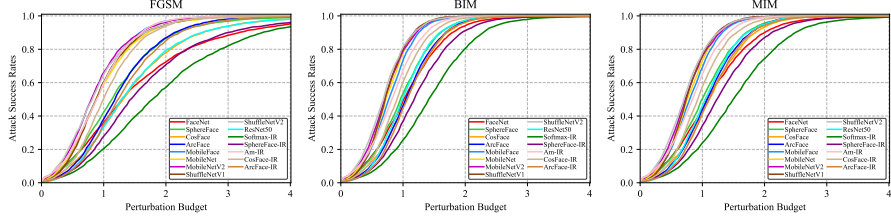


Figure 34: The attack success rate vs. perturbation budget curves of the 15 models against impersonation attacks under the  $\ell_\infty$  norm on CFP-FP.

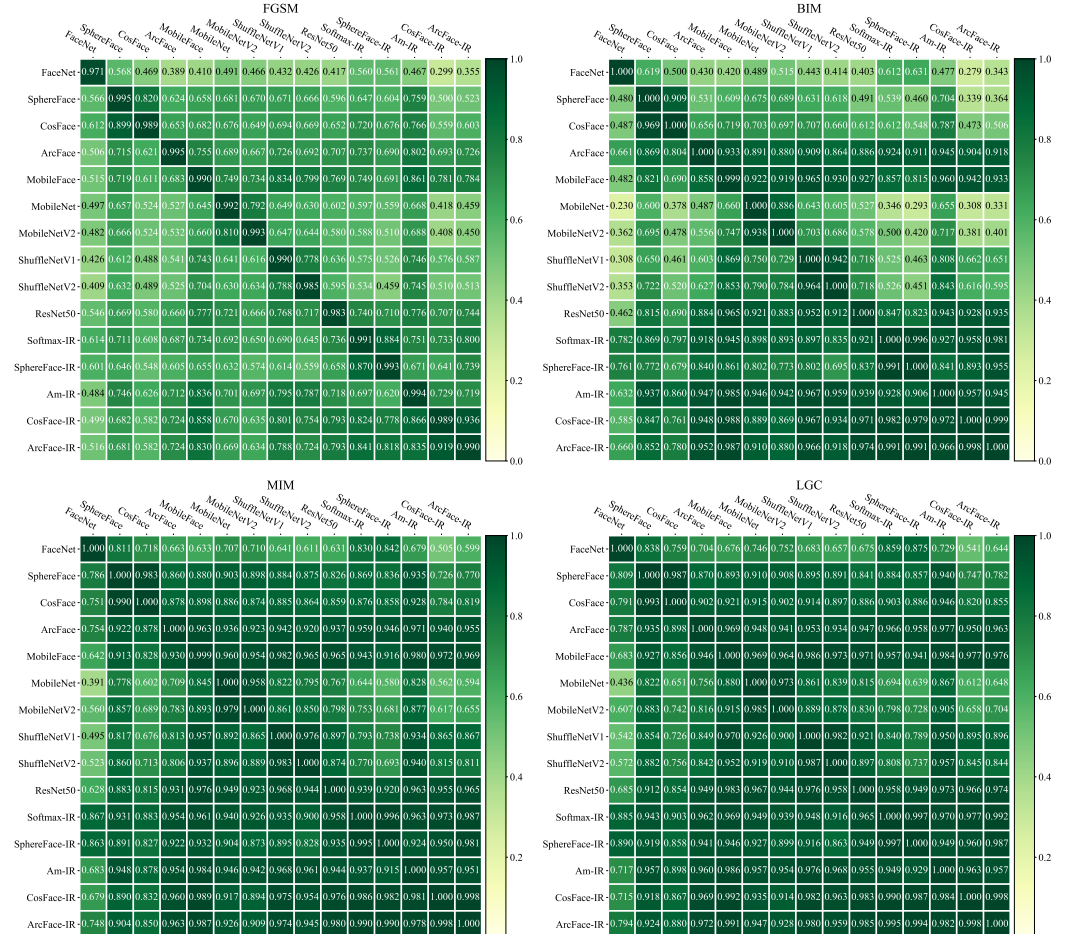


Figure 35: The success rates of the 15 models against black-box dodging attacks under the  $\ell_\infty$  norm on MegFace.

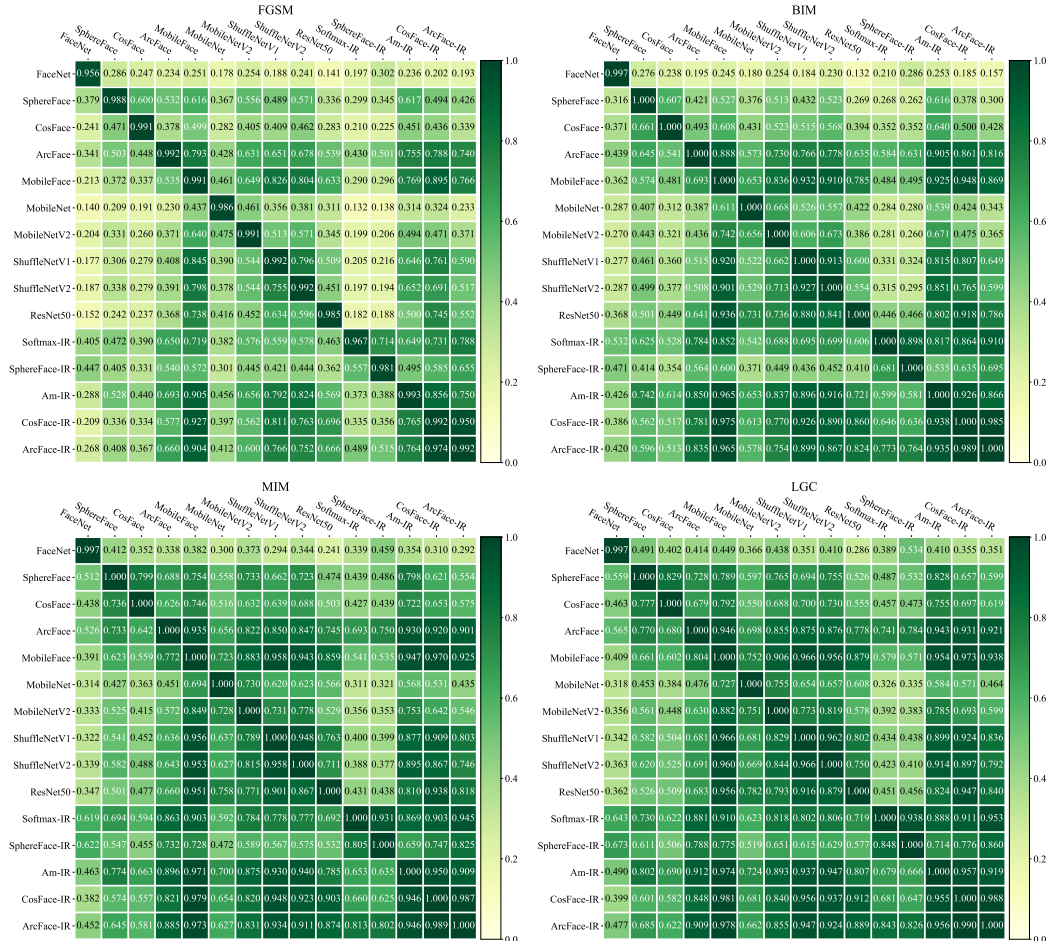


Figure 36: The success rates of the 15 models against black-box impersonation attacks under the  $\ell_\infty$  norm on MegFace.